NACA RM A51J10

NACA

RESEARCH MEMORANDUM

AN INVESTIGATION OF THE CONTROL-SURFACE FLUTTER DERIVATIVES OF AN NACA 65_1-213 AIRFOIL IN THE AMES 16-FOOT HIGH-SPEED WIND TUNNEL

By John A. Wyss and Robert M. Sorenson

Ames Aeronautical Laboratory
Moffett Field, Calif.

NATIONAL ADVISORY COMMITTEE
FOR AERONAUTICS

WASHINGTON

December 21, 1951
Declassified October 31, 1958

NATIONAL ADVISORY COMMITTEE FOR AERONAUTICS

RESEARCH MEMORANDUM

AN INVESTIGATION OF THE CONTROL-SURFACE FLUTTER DERIVATIVES OF AN NACA 65_1-213 AIRFOIL IN THE AMES 16-FOOT HIGH-SPEED WIND TUNNEL

By John A. Wyss and Robert M. Sorenson

SUMMARY

Control-surface flutter derivatives were determined for a sinusoidally oscillating control surface mounted on a two-dimensional fixed airfoil for a range of reduced frequency based on the semichord from 0.05 to 2.00 for two angles of attack, 0° and 4°. The model had an NACA 65_1-213 (a = 0.5) profile, with the control surface hinged at the 75-percent-chord position. For Mach numbers less than the critical, the magnitudes of the resultant hinge-moment coefficients were in reasonable agreement with the value predicted by the theory of Theodorsen (NACA Rep. 496, 1935). Phase angles, however, were consistently smaller. For Mach numbers greater than 0.4, the discrepancy in phase angle resulted in imaginary components of the hinge-moment coefficients which were of opposite sign from those predicted by the theory. For supercritical Mach numbers, large values of negative aerodynamic damping were found for values of reduced frequency from 0.20 to 0.40 for Mach numbers more than 0.06 above the Mach numbers for lift divergence. This implication of a self-excited oscillation and single-degree-of-freedom type of flutter was confirmed by the existence of free flutter of the control surface, self-excited oscillations occurring near 0.75 and 0.80 Mach numbers for 4° and 0° angles of attack, respectively.

INTRODUCTION

Previous investigations of the single-degree-of-freedom type of flutter have established qualitative relations between flow separation, shock-wave motion, and control-surface instability at speeds above the critical. (See references 1 to 3.) Since data presented in these references were obtained primarily during unrestrained control-surface oscillation, quantitative hinge-moment data were limited to the critical speeds and to the frequencies of free flutter. The present investigation was undertaken to determine systematically the experimental hinge-moment coefficients for a wide range of frequencies and Mach numbers

as well as for those particular conditions at which free flutter occurs. In this manner, it was hoped a better understanding of the effects of compressibility at transonic speeds could be obtained. Also, a direct comparison could be made with existing theories such as those developed by Theodorsen (reference 4) and Dietze (reference 5), based on incompressible and compressible flow, respectively. In addition, a comparison could be made with a previous investigation at low speeds reported in reference 6.

To accomplish these purposes, an investigation of the aerodynamic hinge moments on a sinusoidally oscillating control surface mounted on a two-dimensional fixed airfoil was conducted in the Ames 16-foot high-speed wind tunnel. The model used had the NACA 65_1-213 (a = 0.5) profile with a round-nosed control surface hinged at the 75-percent-chord line of the airfoil. The aerodynamic forces acting on the control surface were measured directly through the use of electrical pressure cells flush with the airfoil surface and an electrical summing circuit which enabled the direct recording of the total aerodynamic hinge moment. The control surface was driven at frequencies from 5 to 37 cycles per second at Mach numbers from 0.2 to 0.8, which corresponded to a range of reduced frequency based on the airfoil semichord from 0.05 to 2.0. The corresponding range of Reynolds number, for this investigation, based on the airfoil chord was from 5 to 11 million.

NOTATION

Coefficients and Symbols

b semichord of airfoil, feet

c_f control-surface chord, feet

h_δ section control-surface hinge moment per unit flap deflection, foot pounds per radian

i $\sqrt{-1}$

K reduced frequency $\left(\frac{\omega b}{V}\right)$

$\frac{1}{K}$ reduced velocity, reciprocal of reduced frequency

M free-stream Mach number

M_{LD} lift-divergence Mach number

q free-stream dynamic pressure, pounds per square foot

V velocity of free stream, feet per second

c_{h_δ} section control-surface hinge-moment coefficient per radian ($c_{h_{\delta_r}} + ic_{h_{\delta_i}} = h_\delta/qc_f^2$)

$c_{h_{\delta_r}}$ real component of section control-surface hinge-moment coefficient per radian, in phase with flap position

$c_{h_{\delta_i}}$ imaginary component of section control-surface hinge-moment coefficient per radian, or aerodynamic damping, in phase with flap velocity

α angle of attack of airfoil relative to free stream, degrees

δ angular displacement of control surface relative to airfoil chord, radians

θ phase angle between control-surface displacement and resultant control-surface hinge moment, degrees

ρ mass density of air, slugs per cubic foot

ω control-surface circular frequency, radians per second

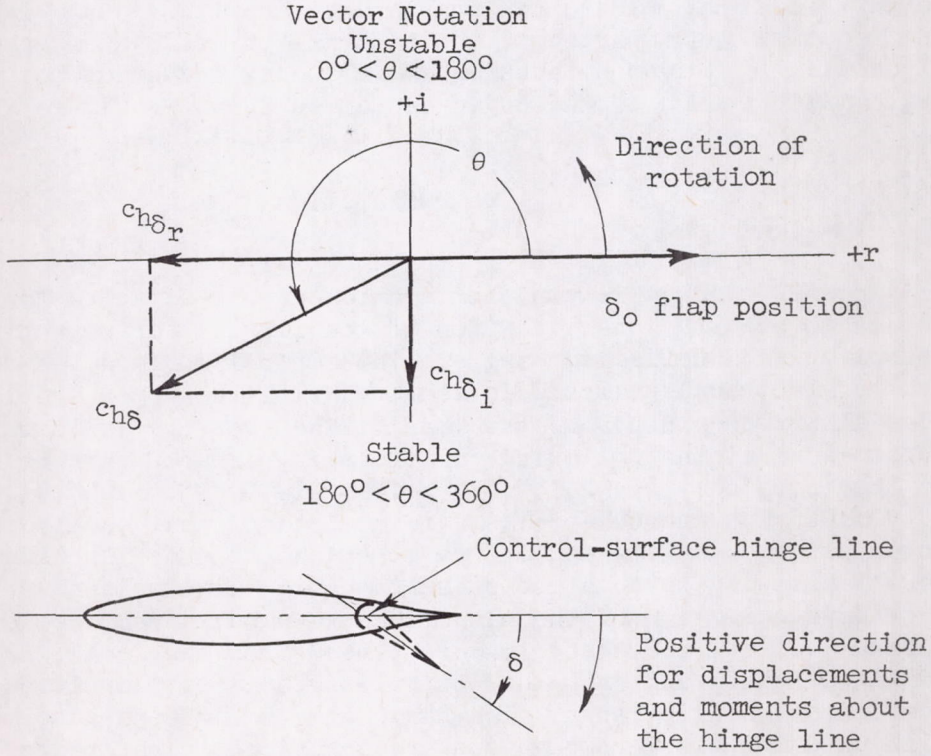

APPARATUS AND METHOD

Tunnel, Model, and Control-Surface Drive

Two walls approximately 16 feet high and 20 feet long were installed 18-1/2 inches apart in the Ames 16-foot high-speed wind tunnel to form a two-dimensional test section. A photograph of the model mounted between these walls is shown in figure 1(a). In figure 1(b) is shown the control-surface oscillator and drive motor mounted on top of the tunnel, with some of the electronic equipment used for the instrumentation shown in the foreground.

The model, constructed of wood and aluminum, had a chord of 4 feet, the NACA 65_1-213 (a = 0.5) profile, and an 18-1/8-inch span. The control surface had a chord length equal to 25 percent of the airfoil chord and was of the round-nosed, unsealed type with a 1/64-inch nose gap and no aerodynamic balance. The spaces between the model and the mounting walls were sealed with sponge rubber from the leading edge to the control-surface hinge line.

A sector arm, splined to one end of the control-surface torque tube within one of the walls, was connected to springs above and below the test section. Sinusoidal angular motion with adjustable amplitude and frequency was imparted to the control-surface system by a mechanical oscillator driven by a variable-frequency induction motor. A diagrammatic sketch of the drive system is shown in figure 2.

Instrumentation

An NACA slide-wire position transducer was attached to the sector arm and to the stationary portion of the airfoil for measuring the control-surface deflection angle. The control surface was instrumented with 16 electrical pressure cells flush with the upper and lower surfaces along the midspan of the model. The pressure cells on each surface were at the following positions in terms of percent chord from the leading edge: 79.42, 85.67, 88.91, 91.49, 93.72, 95.71, 97.52, and 99.19. The pressure cells were so located that each cell represented a region having equal area moment about the flap hinge line, thereby allowing computation of aerodynamic hinge moments from direct electronic summation of the electrical responses from the individual pressure cells. The electrical responses from each cell, from the summing circuit, and from the control-surface position transducer were recorded on oscillographs. The basic electronic apparatus and pressure cells used in this investigation are described in reference 7.

Tests

Static calibration of the slide-wire transducer, of the individual pressure cells, and of the summing circuit was made before and after each run. The electrical response of the slide-wire transducer had a linear variation with changes in angle of deflection of the control surface. The pressure cells, which were individually adjusted to equal sensitivity, and the summing circuit were calibrated by visually reading and recording the changes in their electrical responses due to known changes in pressure. These calibrations were also linear. Static calibrations were used since dynamic tests indicated an amplitude response that corresponded to the static calibrations of the pressure cells for the frequency range of the investigation, with no detectable phase errors.

With Mach number and angle of attack constant, oscillograph records for time intervals of about 2 seconds were taken for several frequencies. The control surface was always oscillated about a 0° mean angle with respect to the airfoil with amplitudes of $\pm 3^\circ$. Records were taken with the following range of variables: angle of attack, 0° and 4°; frequency, 5 to 37 cps; Mach number, 0.2 to 0.8. The Reynolds number based on the airfoil chord varied between 5 and 11 million with the variation of Mach number.

The control surface was oscillated in still air and records were made for several frequencies to determine the inertia effects on the pressure-cell diaphragm. The inertia effects were also calculated using the average weight of three different cell diaphragms. A comparison of the calculated and experimental results, reduced to coefficient form, is shown in figure 3 for an assumed free-stream Mach number of 0.75. Similar tests made with each cell capped to isolate the inertia effects from possible effects of air loads gave similar results.

Reduction and Precision of Data

Oscillograph records illustrative of the type of data obtained in this investigation are shown in figure 4. A comparison of figure 4(b) with figure 4(a) indicates the necessity for harmonic analysis of the data due to the nonsinusoidal nature of the pressure fluctuations when the free-stream Mach number was above the critical. The components of the aerodynamic hinge moment in phase with control-surface position and in phase with the control-surface velocity were determined from a harmonic analysis of three consecutive cycles of the control-surface sum circuit and position traces. A correction for the inertia force due

to acceleration of the diaphragm determined from the runs made in still air was applied to the hinge-moment component in phase with position. Only the hinge moments of the fundamental frequency from the harmonic analysis were used since it has been shown that a harmonic force with a frequency different from that of the motion does zero net work in a time interval which includes an integral number of cycles of both force and motion. (See reference 8.)

The data were not corrected for wind-tunnel-wall effects. The magnitudes of tunnel-wall corrections calculated from reference 9, which included noncirculatory as well as circulatory terms of the theoretical coefficients, were found to be less than the experimental scatter of the reduced data. The calculated correction effectively reduced the resultant hinge-moment coefficient by less than 5 percent at a reduced frequency of 0.075, and by less than 1.0 percent as the reduced frequency increased to 0.80 with little or no change of phase angle. Since there is no presently available analysis of tunnel-wall corrections for oscillating air forces which takes into account the effects of the compressibility of the air, this effect is unknown. However, it is assumed that this effect was relatively minor since corrections based on incompressible flow are so small. End effects at the model-and-wall junctures are of unknown magnitude but are considered negligible in the present investigation as air forces were measured only along the midspan of the model and it was assumed that the flow was two-dimensional.

The precision of the data presented is primarily dependent upon the error involved in reading the oscillograph records, the accuracy in the determination of calibration constants, and how closely the summation of the individual cell readings represented the actual aerodynamic hinge moment on the control surface.

From the original oscillograph records, it was possible to read amplitudes to an accuracy of 0.010 inch and time to 0.0004 second. At 37 cps, these values correspond to a reading accuracy of about 1.0 percent in amplitude and 1.5 percent in frequency and phase angle, or a maximum possible phase-angle error of about 5.3°.

The static calibration of the individual cells had an accuracy of ±2 percent. Since the error was random, the precision of the sum-circuit calibration would be expected to fall within this limit. The sum-circuit calibration was found to change slightly during each run, with an average change of ±3 percent; consequently, an average of the calibrations made before and after each run was used in reduction of the data.

To provide a specific indication of the accuracy of the sum circuit, a harmonic analysis was made of the oscillograph traces from

the individual cells and from the sum circuit on a typical record. The magnitude of the hinge moment calculated from the individual cells was within 2 percent of the hinge moment indicated by the sum trace in all harmonics up to the fifth. In addition, the chordwise variation of pressure indicated by the individual cells was plotted for several typical records, and several curves were faired through the points for each pressure distribution. Integration of the various curves showed a deviation of less than 2 percent from the hinge moment indicated by the sum-circuit trace.

The only criterion used in the selection of records to be analyzed was that all pressure cells were functioning properly and that no large change in calibration occurred.

The reduced data from the investigation are tabulated for 0° angle of attack in table I, and for 4° angle of attack in table II.

RESULTS AND DISCUSSION

The results and the discussion have been grouped in two sections: The first is a comparison of results with those of a previous low-speed investigation and with incompressible and compressible-flow theories; the second is concerned with the observed deviations from theory at transonic speeds.

Subsonic Results

Comparison with previous results at low speeds.- The results for 0.2 and 0.4 Mach number are compared in figure 5 with data from a previous investigation at low speeds and 0° angle of attack reported in reference 6. The data shown from the previous investigation are for flap-chord to wing-chord ratios of 0.40 and 0.10, as compared to the 0.25 ratio of the present investigation; and for the same amplitude of oscillation of 3° as of the present results. To present the data for 0.2 and 0.4 Mach numbers in the same form as the commonly used notation of reference 6, the hinge-moment coefficients c_{h_δ} were divided by $8\pi K^2$, and were plotted as a function of reduced velocity $V/\omega b$. In figure 5, and in subsequent figures, the theoretical curves for incompressible-flow theory are values of Theodorsen's aerodynamic moment coefficients derived from reference 4. These are tabulated by Smilg and Wasserman in reference 10.

An examination of figure 5 indicates that the general trends of the measured coefficients were similar for each investigation.

Comparison with incompressible flow theory.- Until a Mach number somewhat greater than the critical was reached, the results were essentially independent of Mach number and are summarized in figure 6. In this figure, and in succeeding figures, the hinge-moment coefficient, the phase angles, and the real and imaginary parts of the hinge-moment coefficients are each plotted as a function of reduced frequency $\omega b/V$. The coefficients are expressed in the notation already in common use for static hinge moments since this form facilitates perception of the physical magnitudes of the flutter derivatives.

In figure 6 the measured magnitudes for the resultant control-surface hinge-moment coefficient were quite close to those predicted by the theory of Theodorsen, while the phase angles were consistently smaller. Since phase angles were so nearly 180°, as shown in figure 6(b), the imaginary parts of the hinge-moment coefficients corresponding to aerodynamic damping were of small magnitudes, as shown in figure 6(d). It is significant to note in figure 6(d) that aerodynamic instability and possibility of single-degree-of-freedom flutter in the absence of mechanical damping is indicated by the presence of small positive values of the imaginary components for all Mach numbers above 0.4.

Comparison with compressible theory.- The measured coefficients for 0.7 Mach number are presented in figure 7. Curves are also presented for theoretical values based on compressible flow which were calculated by Minhinnick in reference 11 using Dietze's method in reference 5. The comparison is made for 0.7 Mach number, since theoretical coefficients are not presently available for other Mach numbers. The measured values of the resultant hinge moment fell below the theoretical values based on compressible flow, but nearly corresponded to the theoretical values based on incompressible flow. However, the increase in the magnitude of the resultant hinge moment indicated by the compressible-flow theory will be seen to occur in subsequent figures for higher Mach numbers for values of reduced frequency from 0.075 to about 0.20. Again, in figure 7(d) the experimental imaginary components are seen to fall below the values predicted by both the incompressible and compressible flow theories and are of opposite sign, indicating the possibility of single-degree-of-freedom flutter.

Transonic Results

Results for supercritical Mach numbers.- The results for Mach numbers of 0.725, 0.75, 0.775, and 0.80 are presented in figures 8 through 11. A study of these figures indicates the sizable effect of

angle of attack on the Mach number at which fundamental changes in the hinge-moment coefficients occur. In particular, a large increase in negative aerodynamic damping for a 4° angle of attack is evident in figure 8 for 0.725 Mach number, while a similar trend is shown for 0° angle of attack in figure 11 for 0.8 Mach number. Since critical Mach numbers determined from reference 12 were 0.51 and 0.70 for 4° and 0° angles of attack, respectively, the occurrence of instability for 4° angle of attack at a lower Mach number may be attributed to the occurrence of shock waves and attendant flow separation at a lower Mach number for this angle of attack as compared to 0°. However, although the theoretical critical Mach number is the free-stream value at which sonic velocity is first attained on any portion of the airfoil, the flow disturbance from the region of supersonic velocity would be expected to be small until lift or/and drag divergence is exceeded. Therefore, the data shown in figures 8 through 11 are compared and discussed in subsequent figures relative to the Mach number for lift divergence since this Mach number is more representative of speeds at which the flow disturbances became significant.

Verification of undamped oscillation with free-oscillation technique.- The results shown in figures 8 through 11 are in qualitative agreement with previous results such as those reported in references 1, 2, 3, and 7. In these previous investigations, it was shown that control-surface oscillation occurred when extensive separation of flow on the airfoil surface was caused by shock waves. A time lag during oscillation between shock-wave and control-surface motion, and therefore an inferred lag of separation effects or lag in readjustment of flow, which could provide a mechanism for negative damping and resultant control-surface oscillation, was described in reference 3. Since negative aerodynamic damping implies an input of aerodynamic energy into the system and the possibility of single-degree-of-freedom flutter, free-flutter tests were made to provide another means of checking the validity of the results of the investigation.

The results from free-flutter runs are given in figures 9 and 11. For these runs, the sector arm of the flap was disconnected from the spring and oscillator system and attached to a hydraulic damper to prevent destruction of the model. With the model at 4° angle of attack, a self-excited oscillation occurred from 0.74 to 0.76 Mach number; and for 0° angle of attack it occurred from 0.79 to 0.81 Mach number. The results obtained during free flutter showed magnitudes similar to the results obtained while the control surface was driven at nearly the same frequencies.

Summary of supercritical results.- To summarize the effects of compressibility for Mach numbers greater than the critical, the resultant hinge-moment coefficients and phase angles are plotted with $M-M_{LD}$

as a parameter in figures 12 and 13 for 0° and 4° angles of attack. The lift-divergence Mach numbers for the test airfoil, determined from unpublished data from the Ames 1- by 3-1/2-foot wind tunnel, were 0.72 and 0.66 for 0° and 4° angles of attack, respectively.

For the moderate angles of attack included in this investigation, it is apparent from figures 12 and 13 that a characteristic change occurred in the trends and magnitudes of the resultant hinge-moment coefficients, along with changes in phase angles at Mach numbers approximately 0.06 above the Mach number for lift divergence. Although the trends of the resultant hinge-moment coefficients for each angle of attack are similar, as indicated by figures 12(a) and 13(a), it can be seen that the trends of the phase-angle curves for 0° angle of attack are different than for 4° angle of attack, with more moderate changes in magnitudes for the smaller angle of attack.

CONCLUDING REMARKS

From an investigation of the control-surface flutter derivatives for the NACA 65_1-213 airfoil with a sinusoidally oscillating flap, the following general observations can be made:

For Mach numbers less than the critical, the magnitudes of the resultant hinge-moment coefficients were in reasonable agreement with those predicted by the theory of Theodorsen. Phase angles were, however, consistently smaller. For Mach numbers greater than 0.4, the discrepancy in phase angle resulted in imaginary components of the hinge-moment coefficients which were of opposite sign from those predicted by the theory.

For Mach numbers exceeding the critical, the trends of the results did not follow the predictions of compressible- or incompressible-flow theory. The experimental coefficients indicated the possibility of a self-excited oscillation or single-degree-of-freedom type of flutter. The existence of negative aerodynamic damping for values of reduced frequency of about 0.3 was confirmed by the existence of free flutter of the control surface. For the moderate angles of attack included in this investigation, marked negative damping appeared at a Mach number approximately 0.06 above the Mach number for lift divergence.

Ames Aeronautical Laboratory
National Advisory Committee for Aeronautics
Moffett Field, Calif.

REFERENCES

1. Erickson, Albert L., and Mannes, Robert L.: Wind-Tunnel Investigation of Transonic Aileron Flutter. NACA RM A9B28, 1949.

2. Perone, Angelo, and Erickson, Albert L.: Wind-Tunnel Investigation of Transonic Aileron Flutter of a Semispan Wing Model with an NACA 23013 Section. NACA RM A8D27, 1948.

3. Erickson, Albert L., and Stephenson, Jack D.: A Suggested Method of Analyzing for Transonic Flutter of Control Surfaces Based on Available Experimental Evidence. NACA RM A7F30, 1947.

4. Theodorsen, Theodore: General Theory of Aerodynamic Instability and the Mechanism of Flutter. NACA Rep. 496, 1935.

5. Dietze, F.: The Air Forces of the Harmonically Vibrating Wing in Compressible Medium at Subsonic Velocity (Plane Problem) Part I. AAF Trans. F-TS-506-RE, November, 1946.

6. Andreopoulos, T. C., Cheilek, H.A., and Donovan, A. F.: Measurements of the Aerodynamic Hinge Moments of an Oscillating Flap and Tab. USAF Tech. Rep. No. 5784, April, 1949.

7. Erickson, Albert L., and Robinson, Robert C.: Some Preliminary Results in the Determination of Aerodynamic Derivatives of Control Surfaces in the Transonic Speed Range by Means of a Flush-Type Electrical Pressure Cell. NACA RM A8H03, 1948.

8. Den Hartog, J. P.: Mechanical Vibrations. McGraw-Hill Book Co., Inc., N. Y., 1947, chs. 1 and 2.

9. Reissner, Eric: Wind Tunnel Corrections for the Two-Dimensional Theory of Oscillating Airfoils. Cornell Aero. Lab., Rep. SB-318-S-3, April 22, 1947.

10. Smilg, B., and Wasserman, Lee S.: Application of Three-Dimensional Flutter Theory to Aircraft Structures. AAF Tech. Rep. No. 4798, July, 1942.

11. Minhinnick, I. T.: Subsonic Aerodynamic Flutter Derivatives for Wings and Control Surfaces (Compressible and Incompressible Flow). Report Structures 87, British R.A.E., July, 1950.

12. Abbott, Ira H., von Doenhoff, Albert E., and Stivers, Louis E., Jr.: Summary of Airfoil Data. NACA Rep. 824, 1945. (Formerly NACA ACR L5C05)

TABLE I.- REDUCED DATA FOR 0° ANGLE OF ATTACK

Forced Oscillations						
M	K	ω	c_{h_δ}	θ	$c_{h_{\delta_i}}$	$c_{h_{\delta_r}}$
0.2	0.305	34.3	-1.073	191.9	-0.222	-1.051
	.595	66.4	-1.091	204.8	-.457	-.990
	.889	99.3	-1.245	203.6	-.498	-1.140
	1.193	133.8	-1.345	214.5	-.761	-1.107
	1.493	167.5	-1.265	217.9	-.778	-.999
	1.763	197.8	-1.396	227.4	-1.031	-.947
	2.157	232.0	-1.783	222.3	-1.203	-1.324
.4	.144	32.2	-.682	189.9	-.118	-.672
	.243	65.5	-.750	188.9	-.113	-.742
	.446	99.6	-.766	191.2	-.150	-.752
	.595	134.5	-.844	193.9	-.204	-.820
	.744	168.3	-.896	194.8	-.229	-.867
	.878	198.6	-.860	196.9	-.251	-.822
	1.015	229.5	-.830	196.8	-.240	-.796
.6	.100	33.9	-.822	183.8	-.067	-.820
	.195	66.6	-.777	175.6	.059	-.776
	.296	100.9	-.816	182.8	-.039	-.815
	.387	132.6	-.791	181.6	-.022	-.791
	.482	164.8	-.797	180.3	.004	-.796
	.583	199.4	-.722	180.9	-.012	-.723
	.667	228.2	-.713	188.0	-.100	-.706
.7	.087	34.5	-.796	176.0	.048	-.795
	.172	68.3	-.774	175.3	.063	-.771
	.257	101.9	-.852	178.8	.018	-.852
	.330	134.5	-.853	173.3	.099	-.847
	.409	165.6	-.798	172.2	.108	-.791
	.423	170.4	-.822	173.4	.094	-.817
	.491	198.6	-.742	176.6	.044	-.741
	.562	228.5	-.753	181.9	-.025	-.753
.725	.083	34.8	-.807	177.9	.025	-.807
	.164	68.1	-.798	181.9	-.027	-.798
	.247	102.9	-.832	182.7	-.039	-.832
	.322	132.8	-.837	178.2	.026	-.837
	.421	164.6	-.811	171.3	.123	-.802
	.461	195.7	-.809	179.0	.014	-.809
	.530	226.0	-.845	183.5	-.051	-.843

TABLE I.- CONCLUDED

Forced Oscillations						
M	K	ω	c_{h_δ}	θ	$c_{h_{\delta_i}}$	$c_{h_{\delta_r}}$
0.75	0.079	34.1	-0.788	182.9	-0.040	-0.787
	.158	68.1	-.773	180.5	-.007	-.773
	.232	102.2	-.824	179.4	.009	-.824
	.300	130.8	-.852	175.7	.064	-.850
	.374	163.4	-.806	175.5	.064	-.803
	.449	195.5	-.797	177.1	.041	-.796
	.521	227.1	-.819	180.1	-.002	-.819
.775	.078	34.8	-.941	180.5	-.008	-.941
	.147	66.4	-.772	171.6	.114	-.763
	.223	100.7	-.860	153.7	.381	-.771
	.302	134.7	-.670	165.2	.171	-.657
	.370	166.7	-.602	174.6	.057	-.599
	.436	194.9	-.718	183.4	-.043	-.717
	.506	226.6	-.702	186.6	-.080	-.697
.80	.073	34.0	-1.134	169.1	.214	-1.112
	.145	67.1	-1.121	155.0	.455	-1.019
	.219	101.5	-1.091	146.5	.602	-.910
	.282	131.4	-1.205	145.7	.680	-.995
	.353	164.9	-.498	137.9	.334	-.370
	.421	196.0	-.848	168.9	.164	-.832
	.490	228.5	-.961	162.7	.286	-.917

Self-Excited Oscillations						
M	K	ω	c_{h_δ}	θ	$c_{h_{\delta_i}}$	$c_{h_{\delta_r}}$
0.805	0.290	135.5	-0.991	129.0	0.770	-0.624
	.303	141.2	-.908	130.0	.695	-.584

TABLE II.- REDUCED DATA FOR 4° ANGLE OF ATTACK

Forced Oscillations						
M	K	ω	c_{h_δ}	θ	$c_{h_{\delta_i}}$	$c_{h_{\delta_r}}$
0.2	0.142	17.1	-1.357	180.9	-0.021	-1.357
	.313	35.1	-1.344	186.5	-.153	-1.336
	.613	68.7	-1.305	202.3	-.495	-1.208
	.925	103.7	-1.456	202.8	-.566	-1.342
	1.193	134.0	-1.553	207.5	-.718	-1.376
	1.485	166.9	-1.620	209.3	-.793	-1.413
	1.780	200.0	-1.640	214.4	-.926	-1.355
	2.068	232.4	-2.181	202.7	-.795	-2.035
.4	.075	17.3	-.832	181.3	-.019	-.832
	.148	34.1	-.811	185.9	-.084	-.807
	.294	68.0	-.814	188.8	-.125	-.810
	.443	102.4	-.831	188.0	-.116	-.824
	.583	133.5	-.944	190.4	-.171	-.930
	.722	165.5	-.987	190.3	-.176	-.972
	.883	199.6	-1.007	191.6	-.203	-.988
	1.031	232.8	-.960	188.6	-.143	-.950
.6	0.046	16.2	-.909	183.4	-.054	-.907
	.095	33.4	-.874	182.4	-.036	-.874
	.193	67.5	-.856	181.5	-.022	-.856
	.289	101.2	-.868	180.4	-.006	-.868
	.380	132.8	-.950	178.7	.022	-.950
	.477	166.5	-.942	177.6	.040	-.941
	.570	198.9	-.923	173.9	.092	-.863
	.657	229.5	-.826	185.0	-.072	-.823
.7	.083	34.1	-.967	172.4	.127	-.959
	.165	67.5	-.870	168.2	.179	-.851
	.246	100.9	-.804	165.8	.198	-.779
	.325	133.0	-.813	171.3	.123	-.804
	.411	168.0	-.868	172.6	.112	-.861
	.486	198.4	-.822	180.6	-.008	-.822
	.501	204.6	-.820	185.5	-.079	-.816
.725	.081	34.1	-1.140	171.0	.180	-1.127
	.159	67.0	-1.160	161.0	.377	-1.096
	.240	101.1	-1.442	142.0	.739	-.946
	.314	132.8	-.607	95.2	.605	-.055
	.392	165.9	-.576	236.1	-.478	-.321
	.466	197.0	-1.023	197.0	-.516	-.883
	.542	229.0	-1.211	198.9	-.390	-1.146

TABLE II.- CONCLUDED

Forced Oscillations						
M	K	ω	c_{h_δ}	θ	$c_{h_{\delta_i}}$	$c_{h_{\delta_r}}$
0.75	0.815	36.1	-1.178	169.6	0.214	-1.159
	.155	68.9	-1.304	162.2	.400	-1.241
	.231	102.5	-1.424	149.9	.712	-1.232
	.312	135.2	-1.194	118.2	1.192	-.064
	.389	168.8	-.566	253.0	-.541	-.165
	.517	228.9	-.750	168.7	.147	-.735
.775	.078	35.6	-1.151	176.8	.065	-1.149
	.150	68.6	-1.197	167.1	.268	-1.166
	.227	103.7	-1.323	155.5	.548	-1.204
	.292	133.7	-.752	130.1	.575	-.484
	.362	165.9	-.664	188.6	-.099	-.657
	.436	199.7	-.961	185.1	-.086	-.957
	.509	233.3	-.744	179.5	.006	-.744
Self-Excited Oscillations						
M	K	ω	c_{h_δ}	θ	$c_{h_{\delta_i}}$	$c_{h_{\delta_r}}$
0.74	0.281	122.0	-1.095	110.6	1.025	-0.385
.74	.286	124.4	-1.099	110.0	1.033	-.375
.75	.293	128.0	-1.208	109.5	1.139	-.403

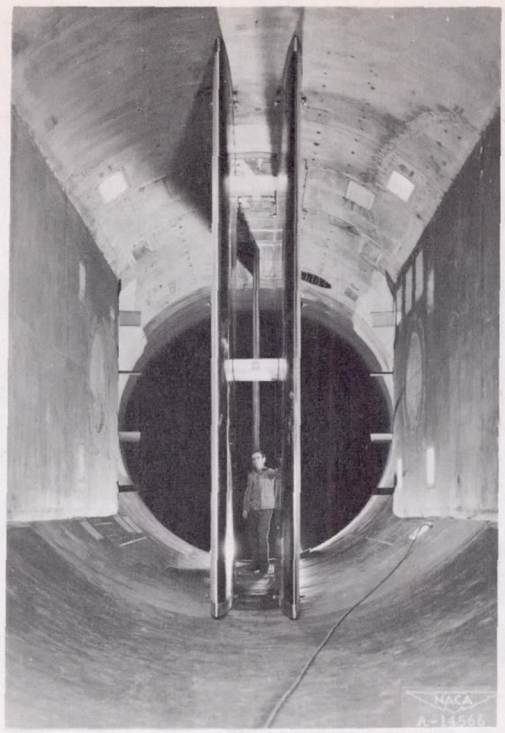

(a) Model mounted between two-dimensional walls.

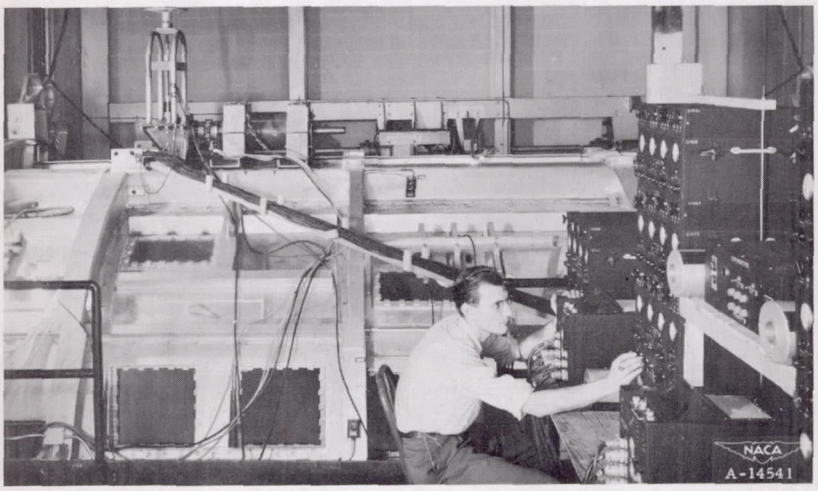

(b) Flap oscillator and drive motor mounted on top of wind tunnel, with electronic equipment in foreground.

Figure 1.- General views of wind-tunnel test section and associated equipment.

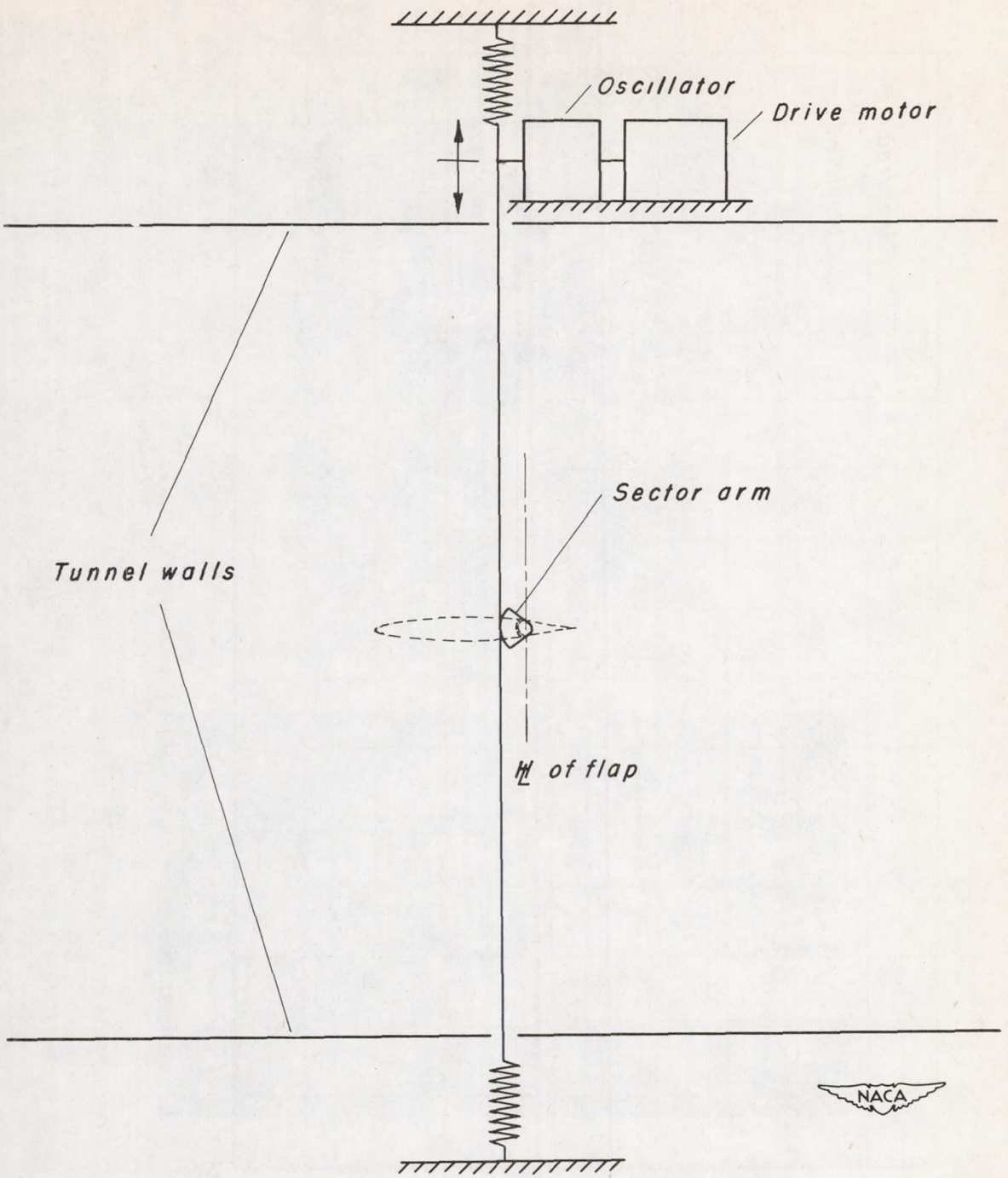

Figure 2.- Diagrammatic sketch of flap drive system.

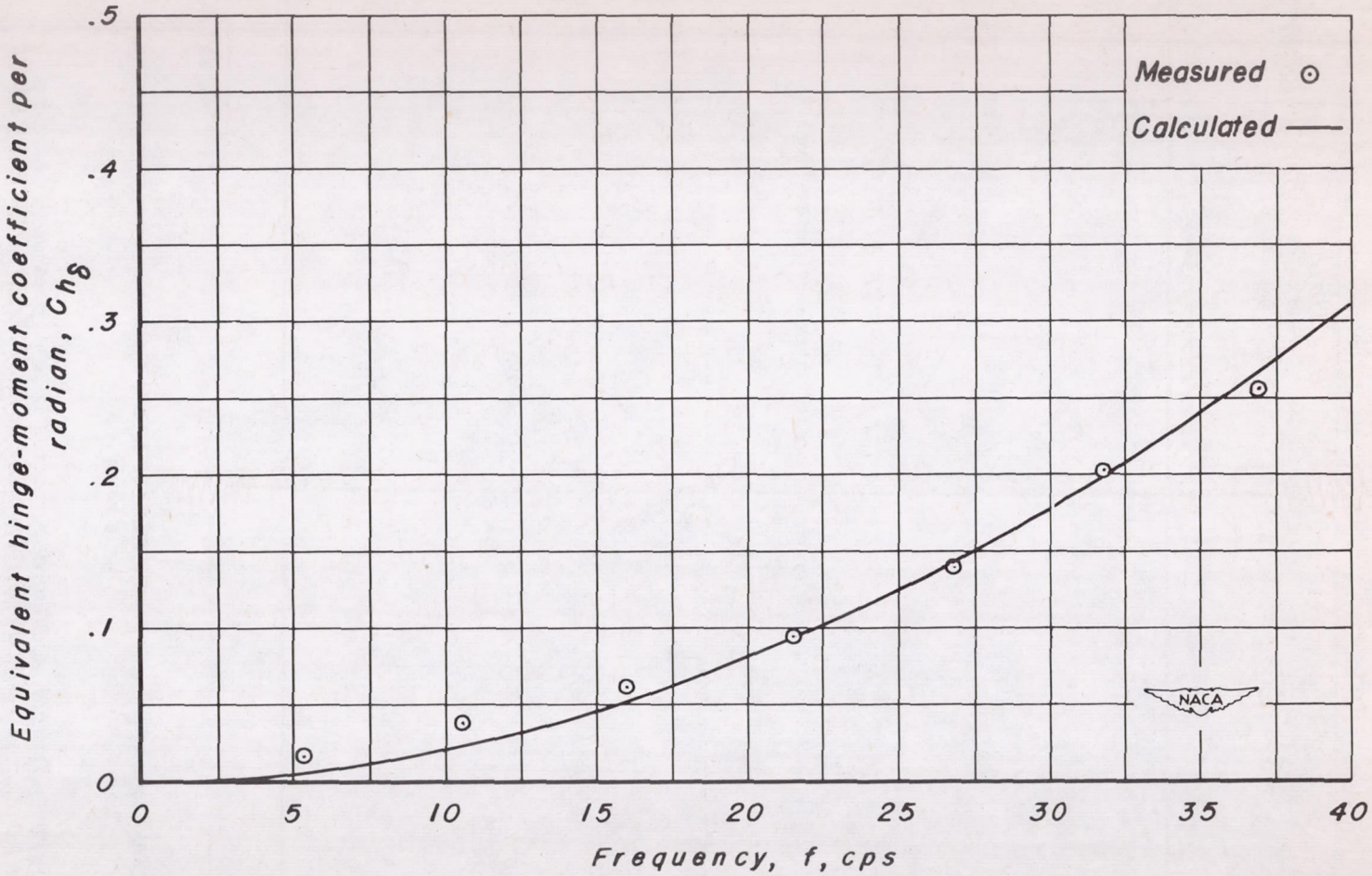

Figure 3.—Comparison of measured and calculated equivalent hinge-moment coefficients due to inertia forces on pressure cell diaphragm for 0.75 Mach number.

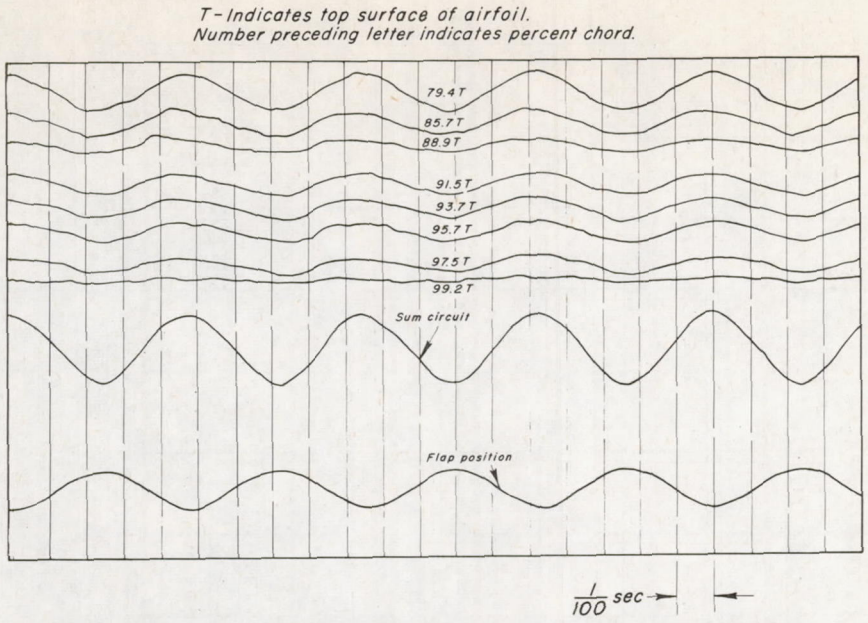

(a) Flap oscillating at 21.13 cycles per second through an included angle of 5.7°. M,0.40

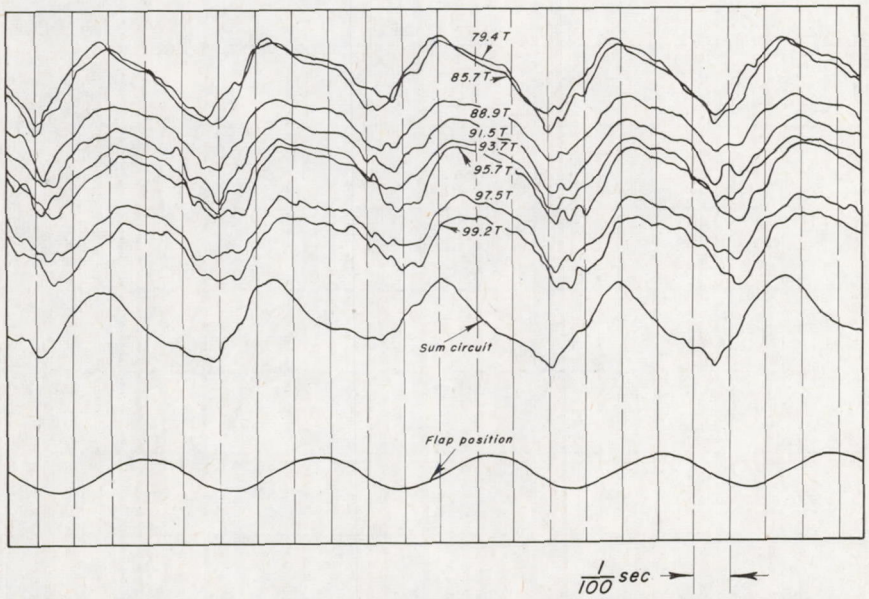

(b) Flap oscillating at 21.14 cycles per second through an included angle of 4.7°. M,0.725

Figure 4.–Typical oscillograph records of the pressure fluctuations on the flap of the NACA 65$_1$-213 airfoil. α, 4°

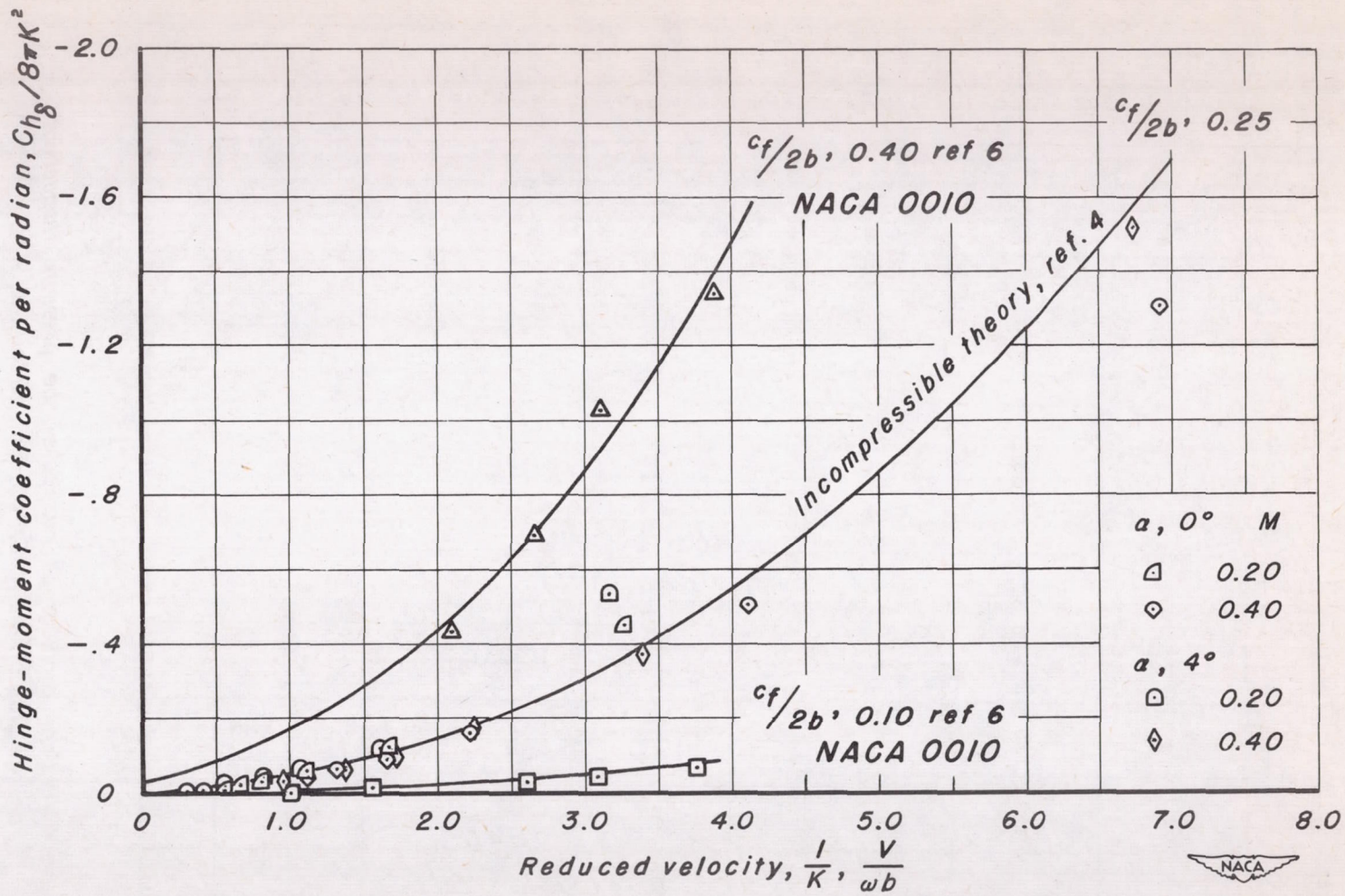

(a) Hinge-moment coefficient as a function of reduced velocity.

Figure 5.— Comparison of low speed control-surface flutter derivatives for NACA 65_1-213 and NACA 0010 airfoils.

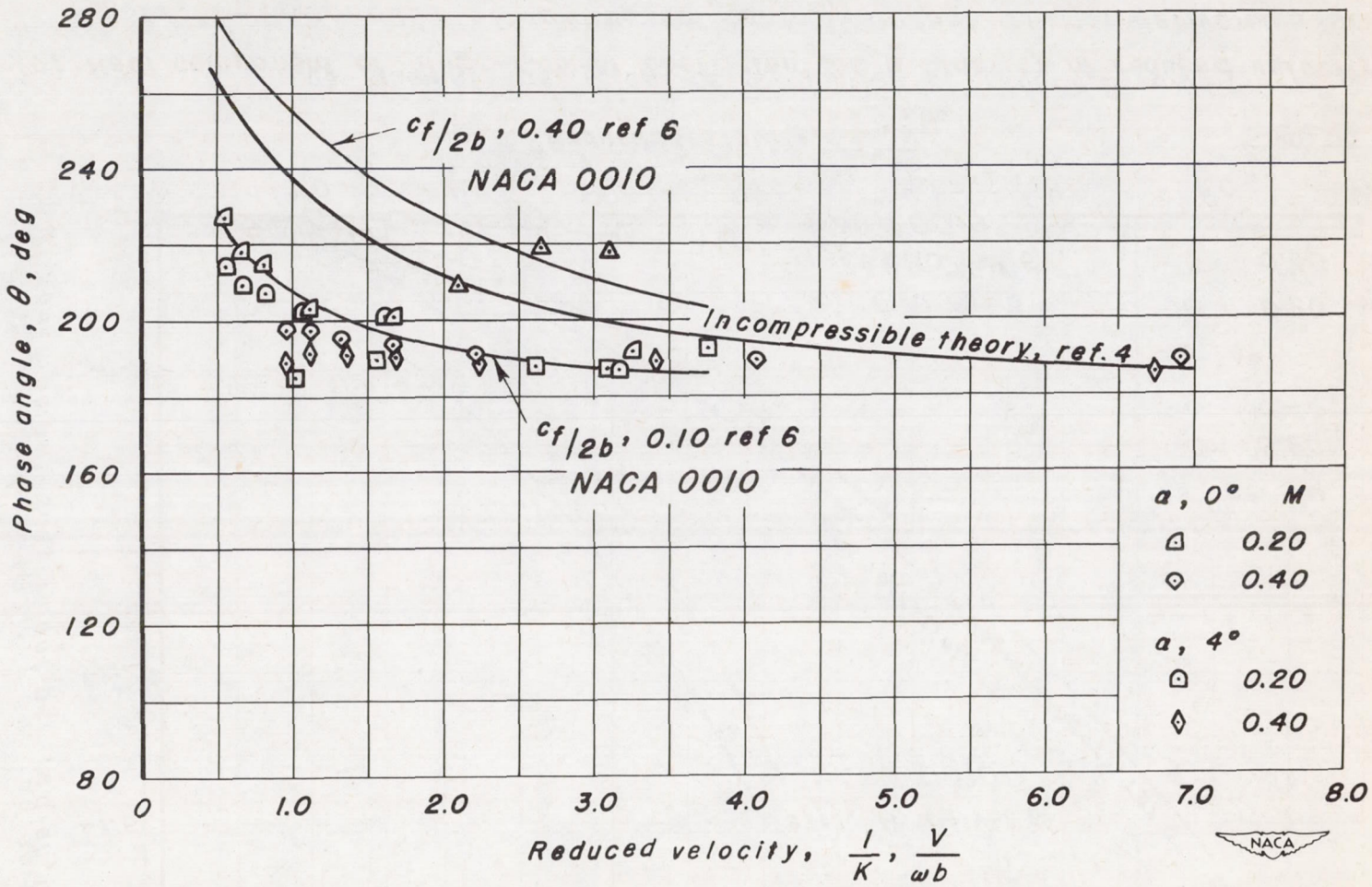

(b) Phase angle of hinge-moment coefficient as a function of reduced velocity.

Figure 5.- Continued.

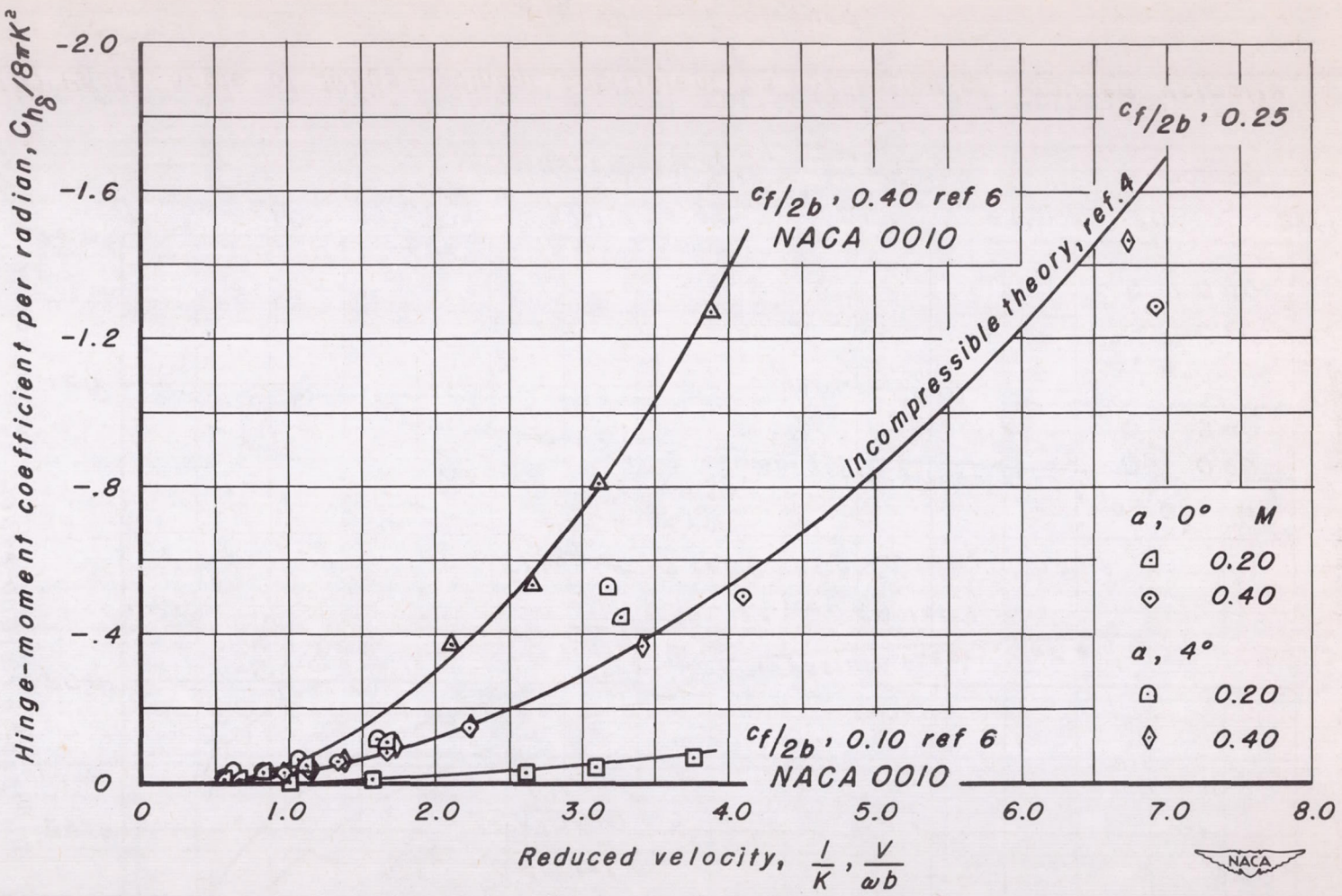

(c) Real component of hinge-moment coefficient as a function of reduced velocity.

Figure 5.- Continued.

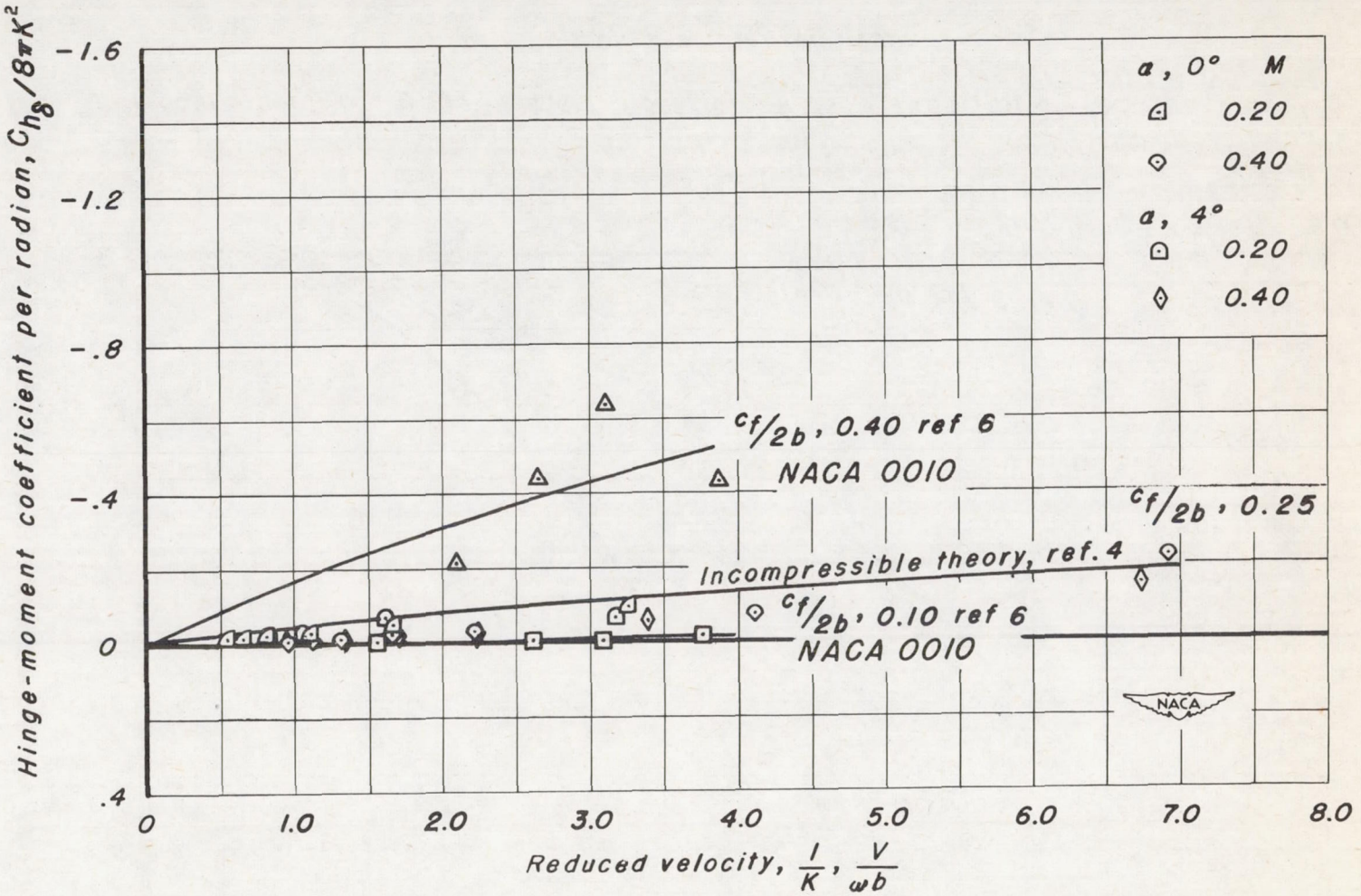

(d) Imaginary component of hinge-moment coefficient as a function of reduced velocity.

Figure 5.—Concluded.

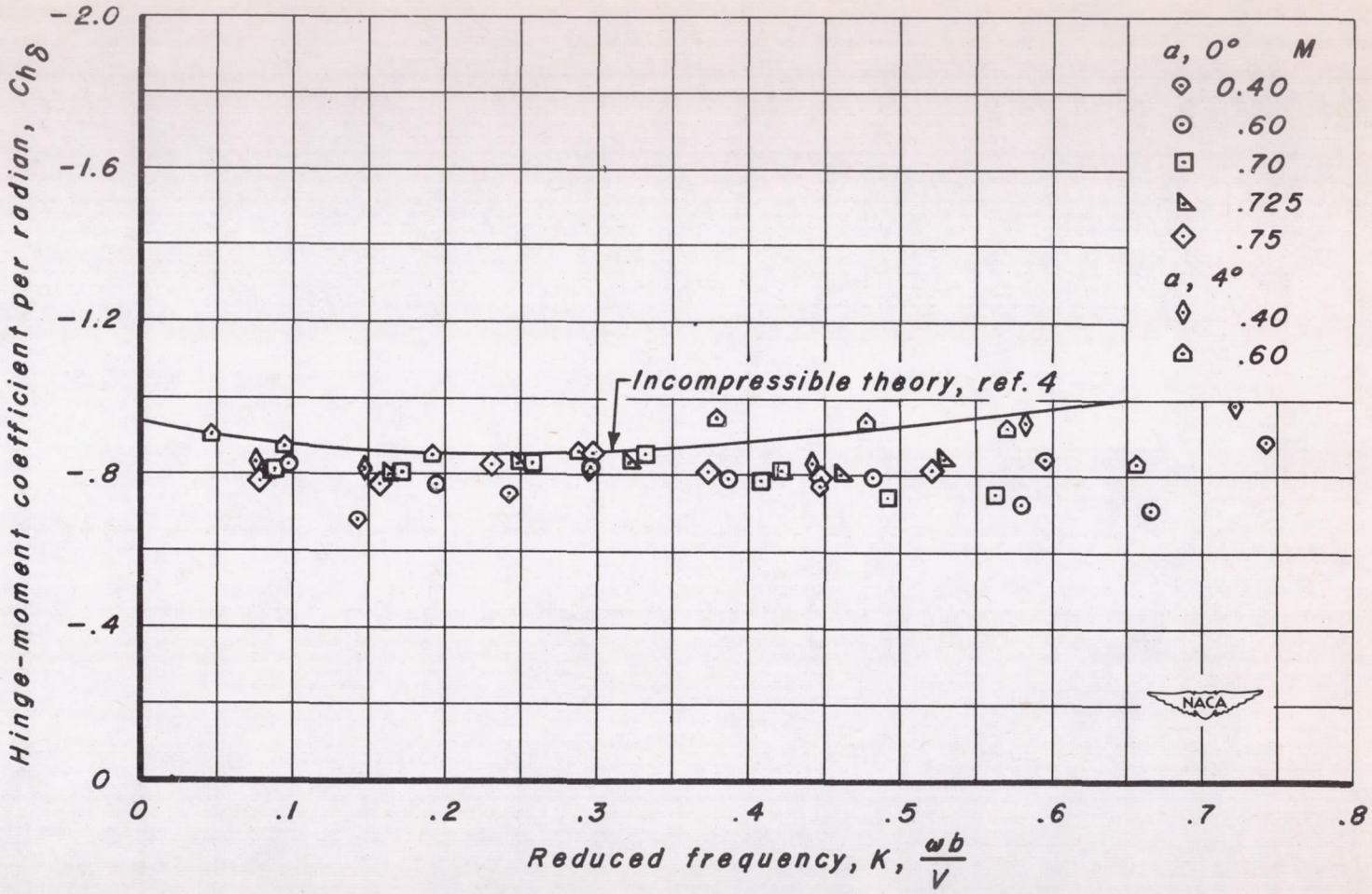

(a) Hinge-moment coefficient as a function of reduced frequency.

Figure 6.- Comparison of control-surface flutter derivatives for NACA 65_1-213 airfoil with incompressible flow theory. a, 0°, 4°

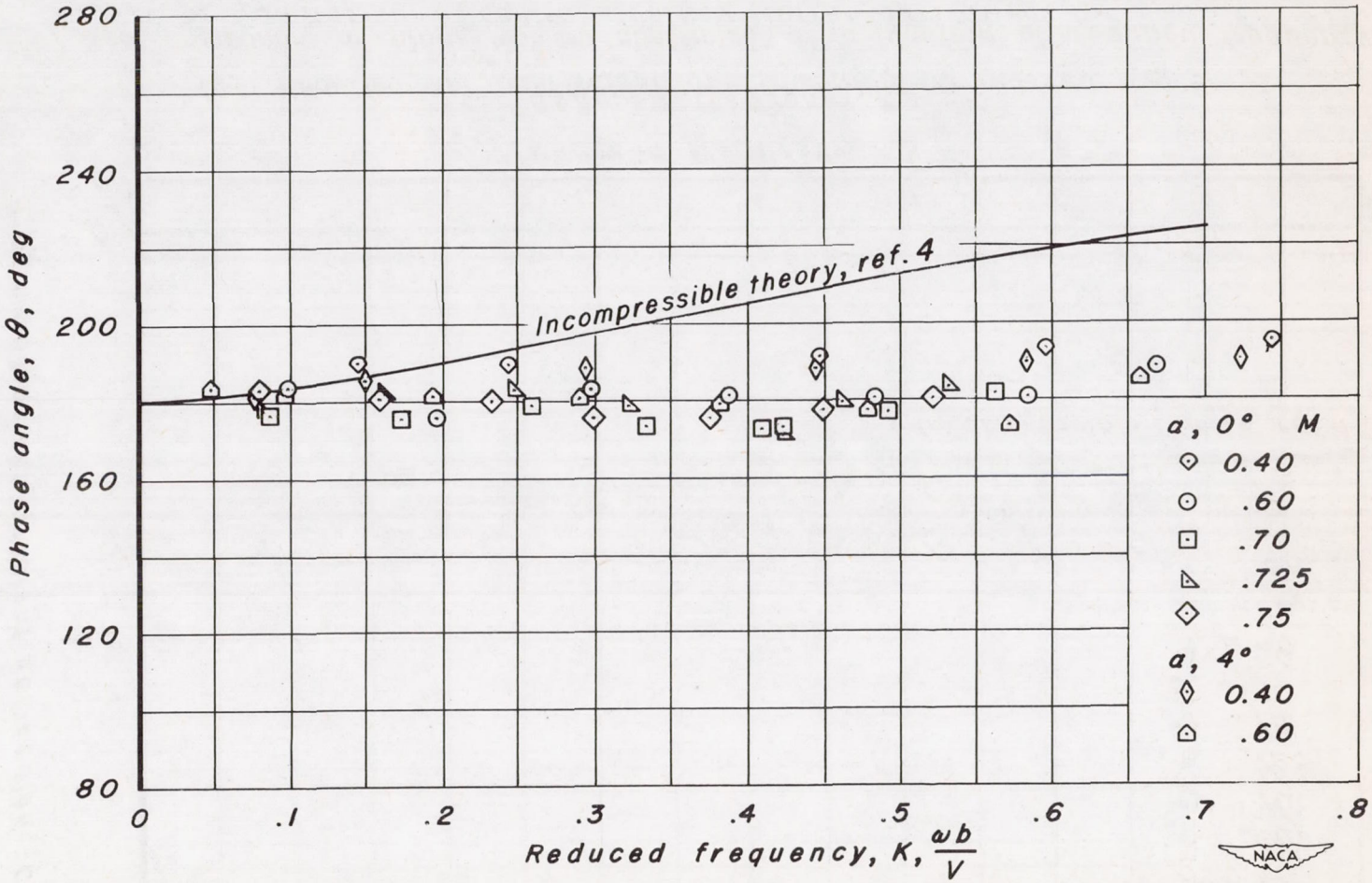

(b) Phase angle of hinge-moment coefficient as a function of reduced frequency.

Figure 6.—Continued.

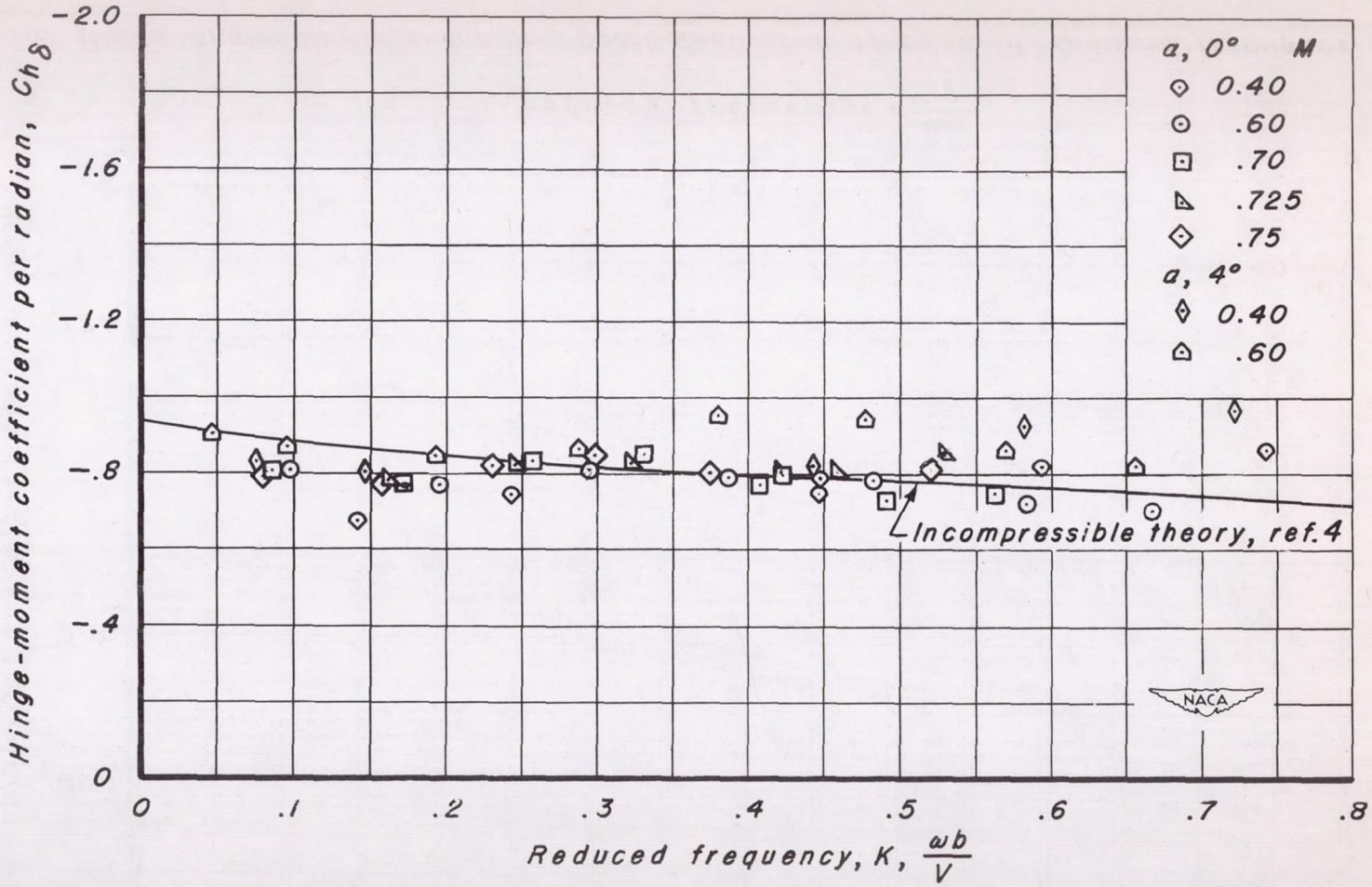

(c) Real component of hinge-moment coefficient as a function of reduced frequency.

Figure 6.—Continued.

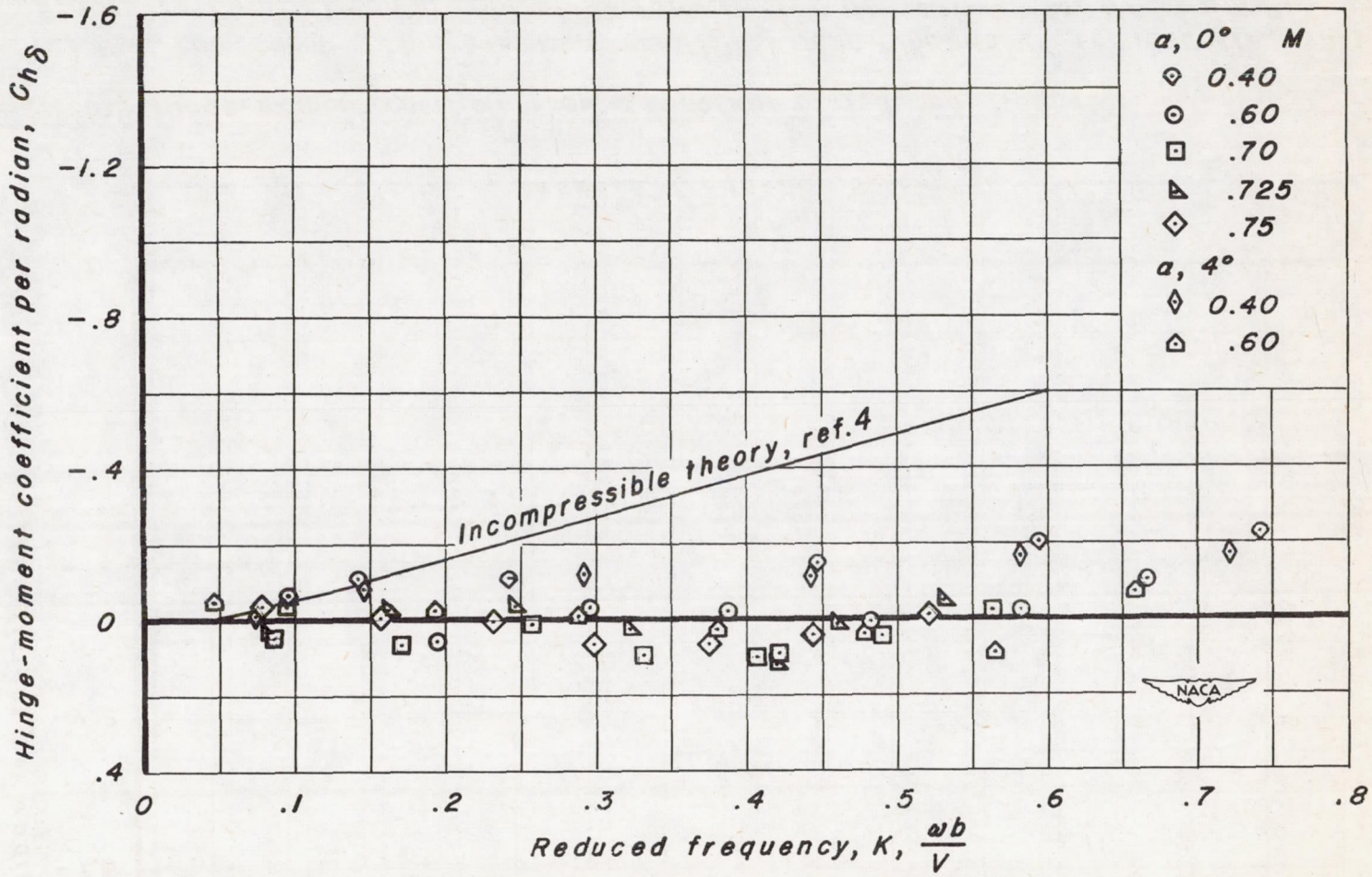

(d) Imaginary component of hinge-moment coefficient as a function of reduced frequency.

Figure 6.—Concluded.

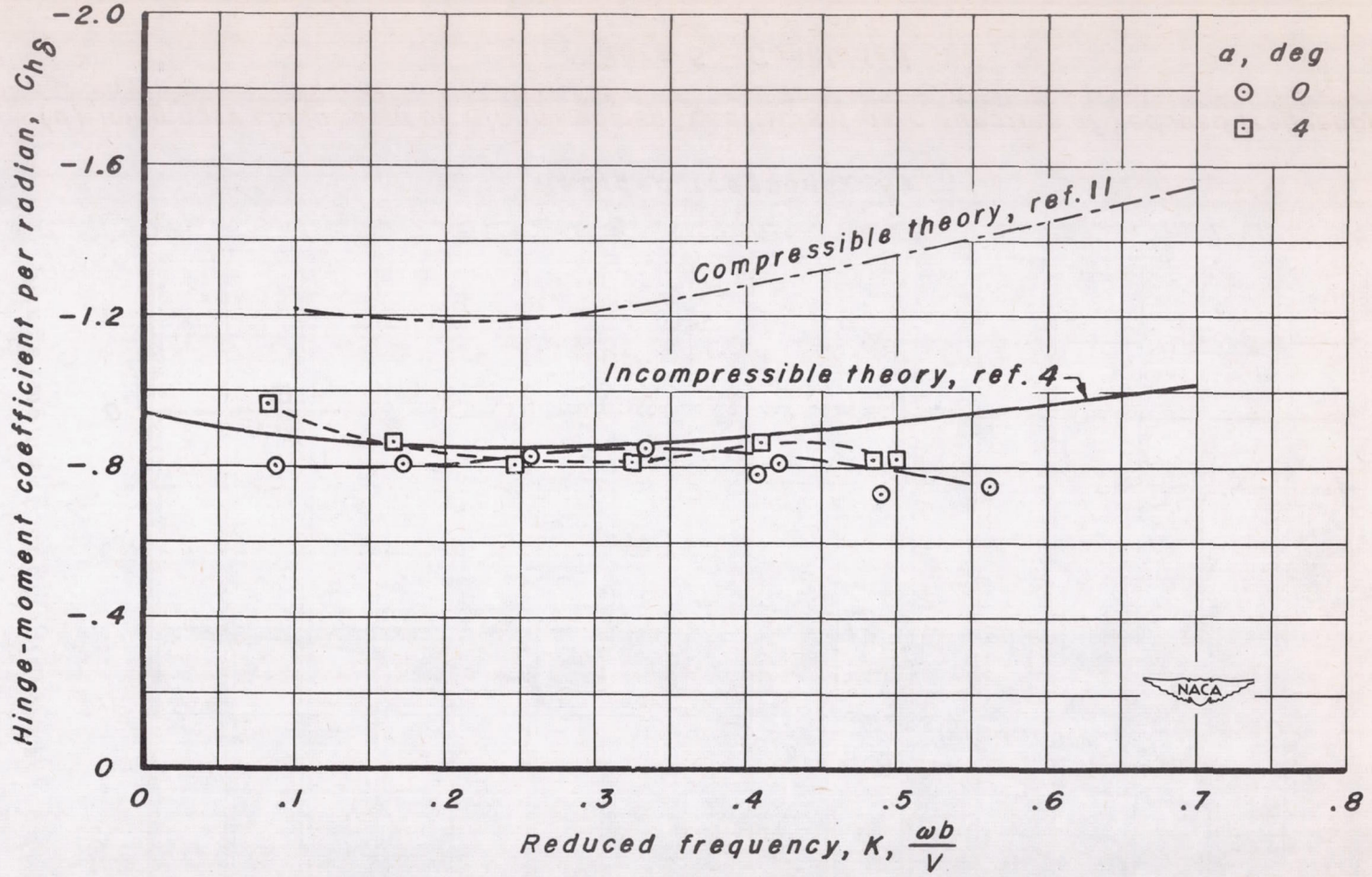

(a) Hinge-moment coefficient as a function of reduced frequency. M,0.70

Figure 7.–Comparison of control-surface flutter derivatives for NACA 65_1-213 airfoil with compressible and incompressible flow theory. a, 0°, 4°

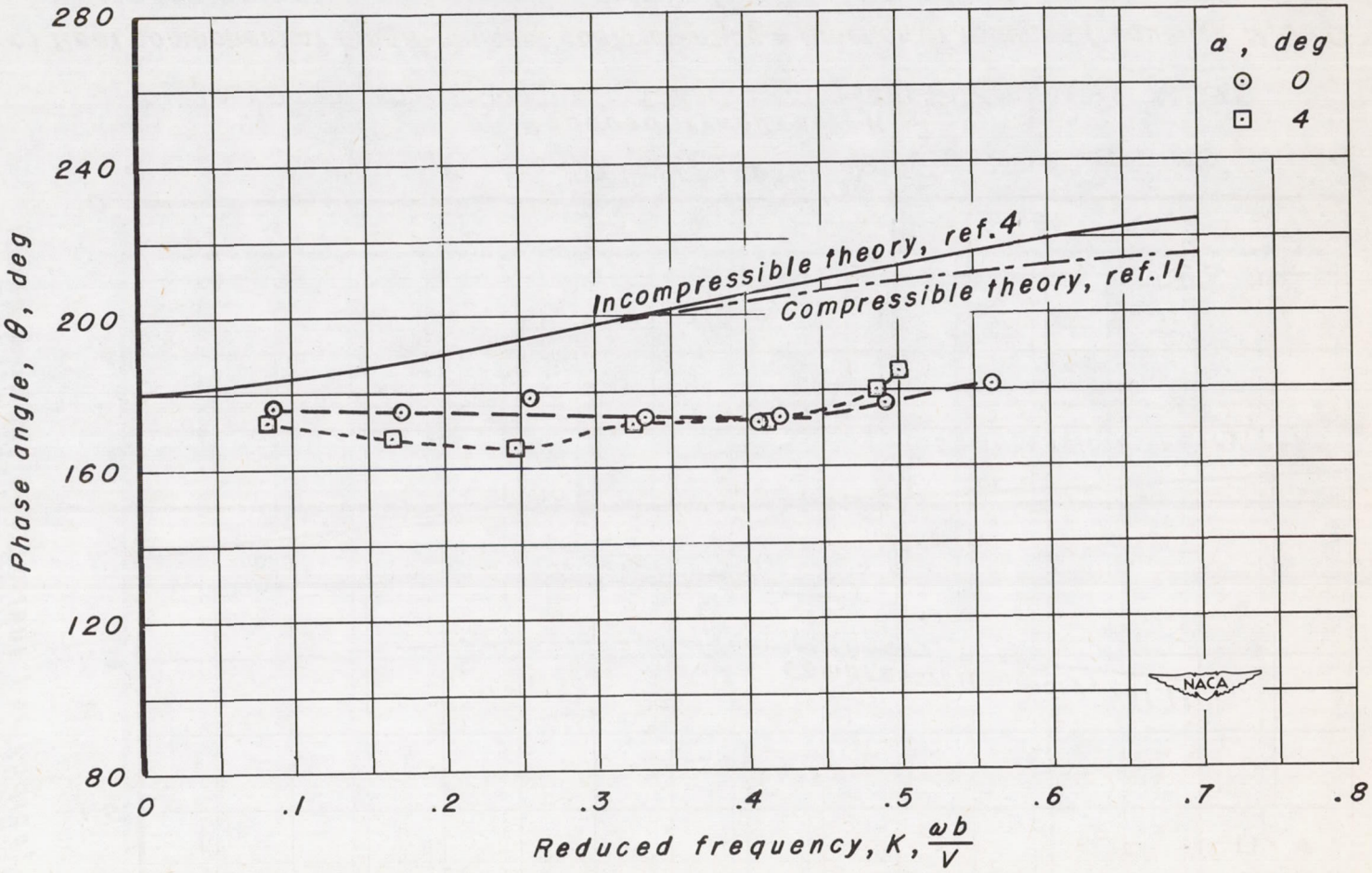

(b) Phase angle of hinge-moment coefficient as a function of reduced frequency. M, 0.70

Figure 7.—Continued.

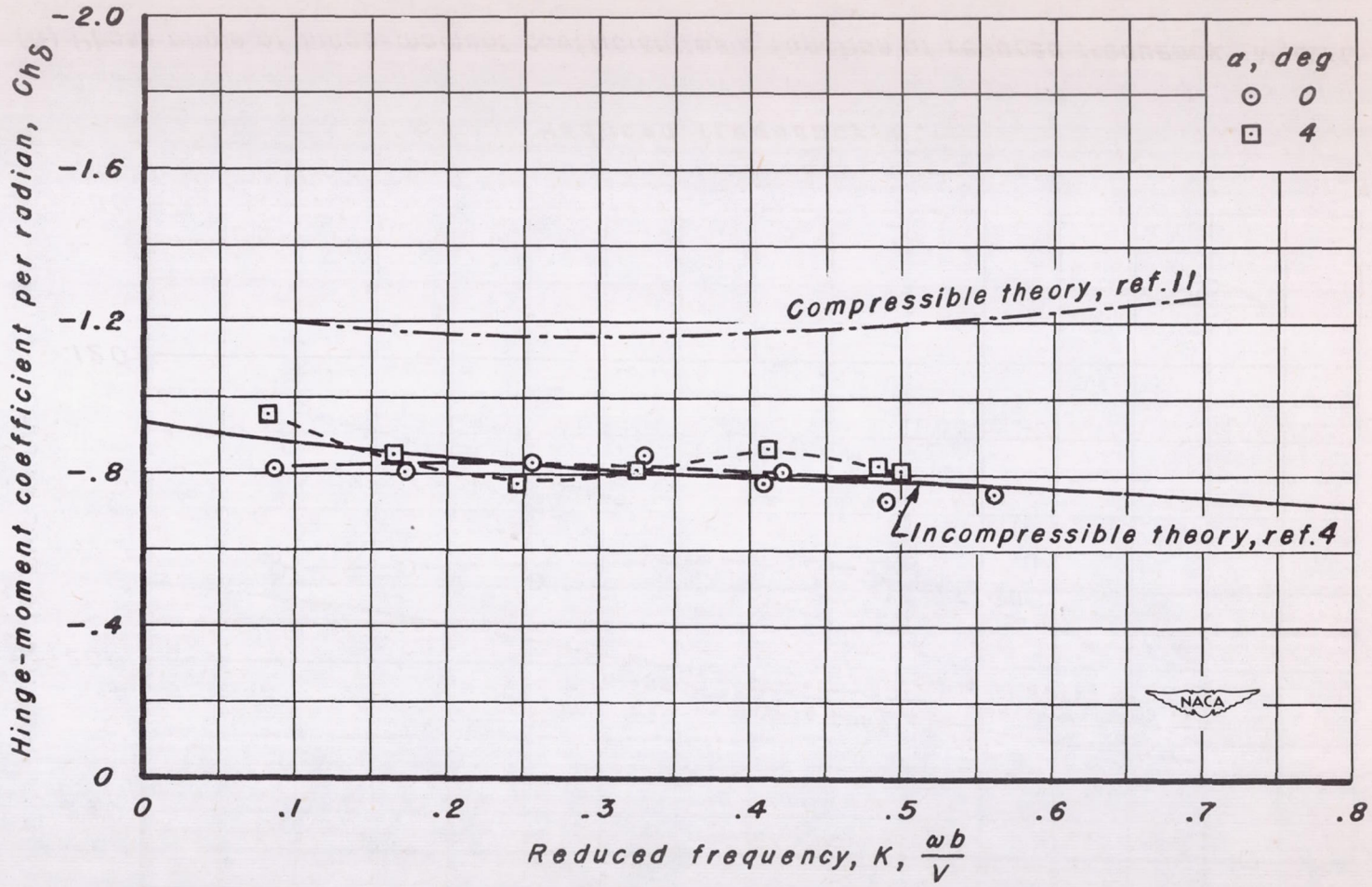

(c) Real component of hinge-moment coefficient as a function of reduced frequency. M, 0.70

Figure 7.–Continued.

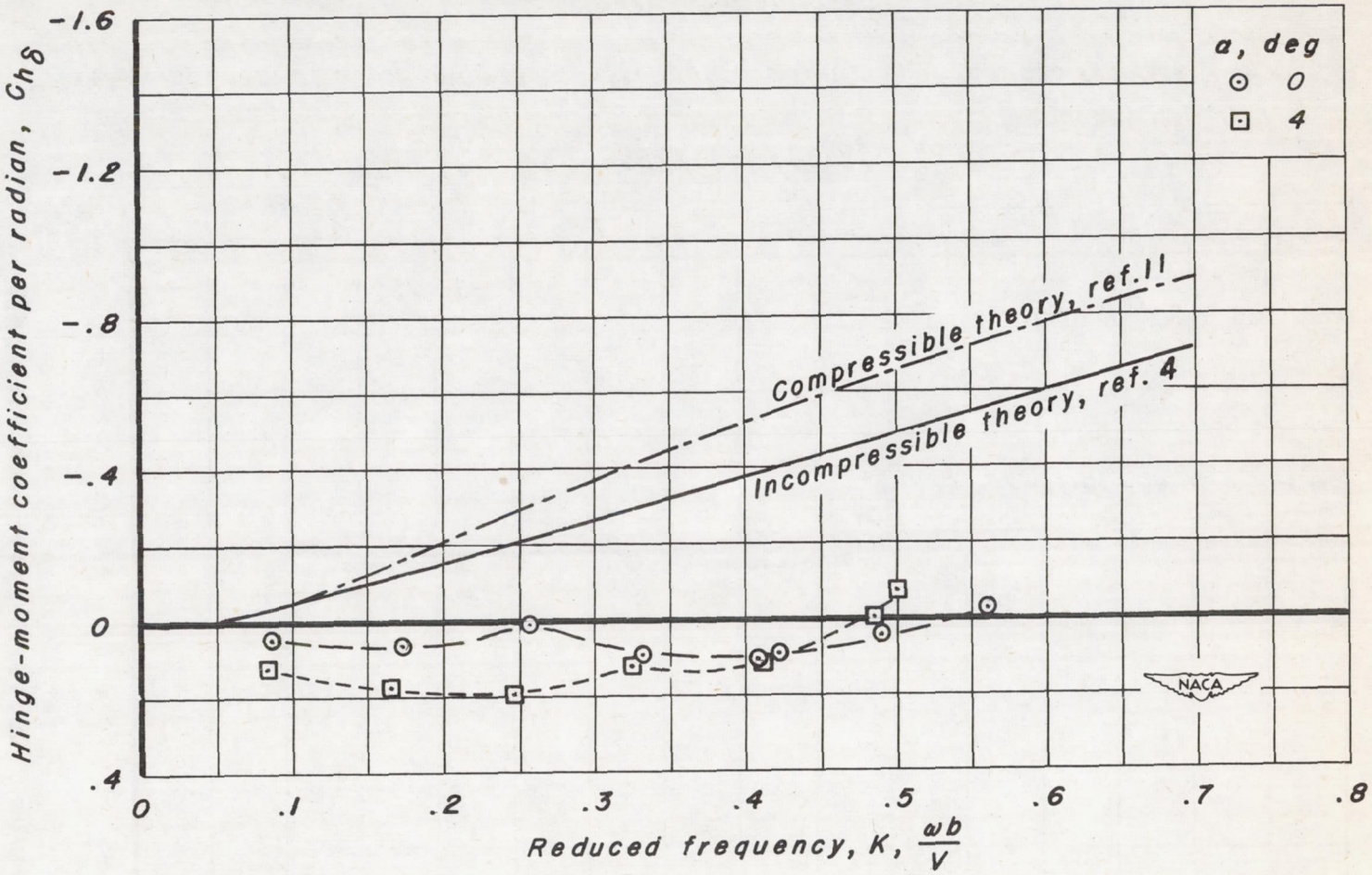

(d) Imaginary component of hinge-moment coefficient as a function of reduced frequency. M, 0.70

Figure 7.—Concluded.

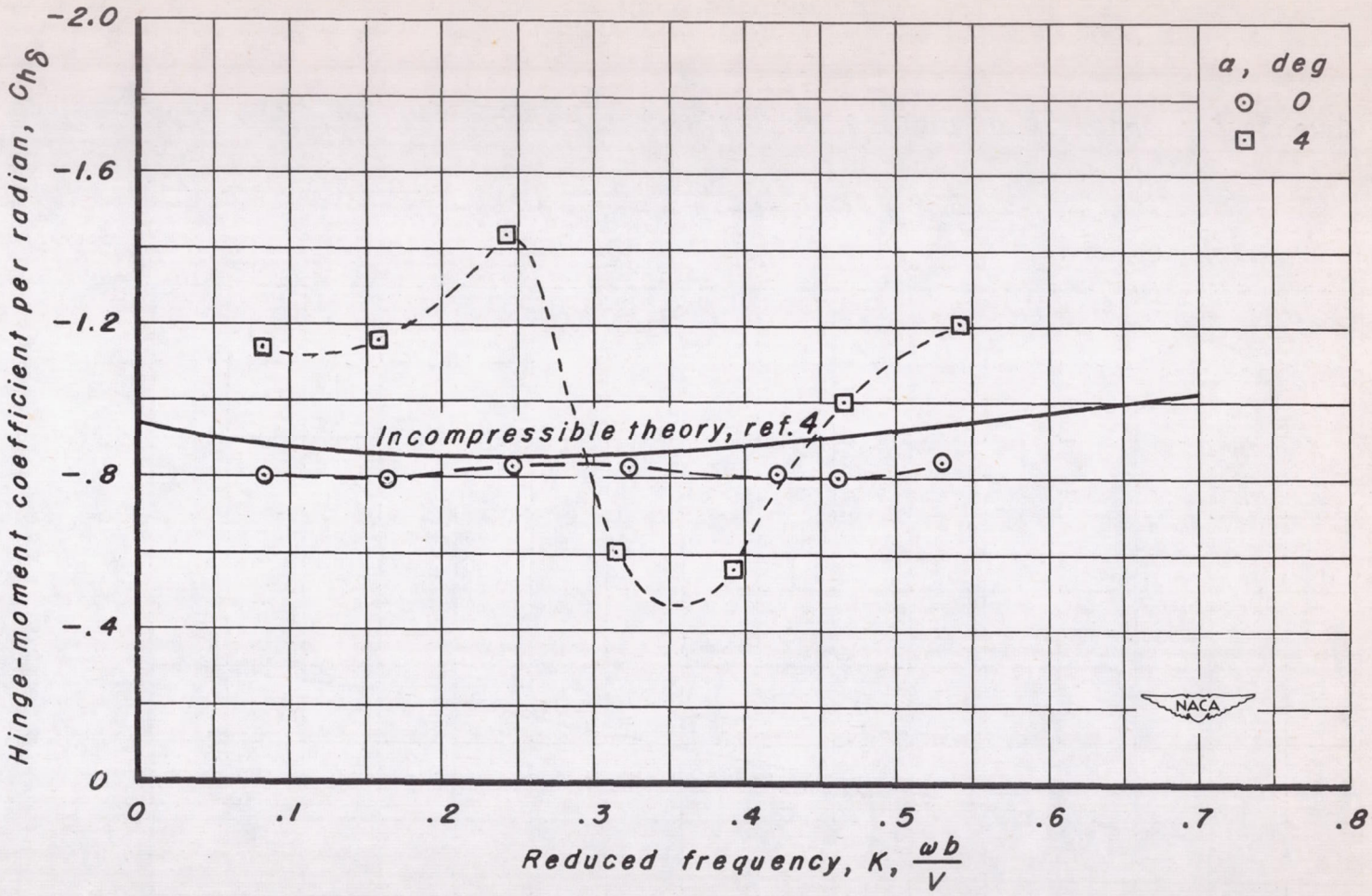

(a) Hinge-moment coefficient as a function of reduced frequency. M,0.725.

Figure 8.—Supercritical control-surface flutter derivatives for NACA 65_1-213 airfoil. M, 0.725

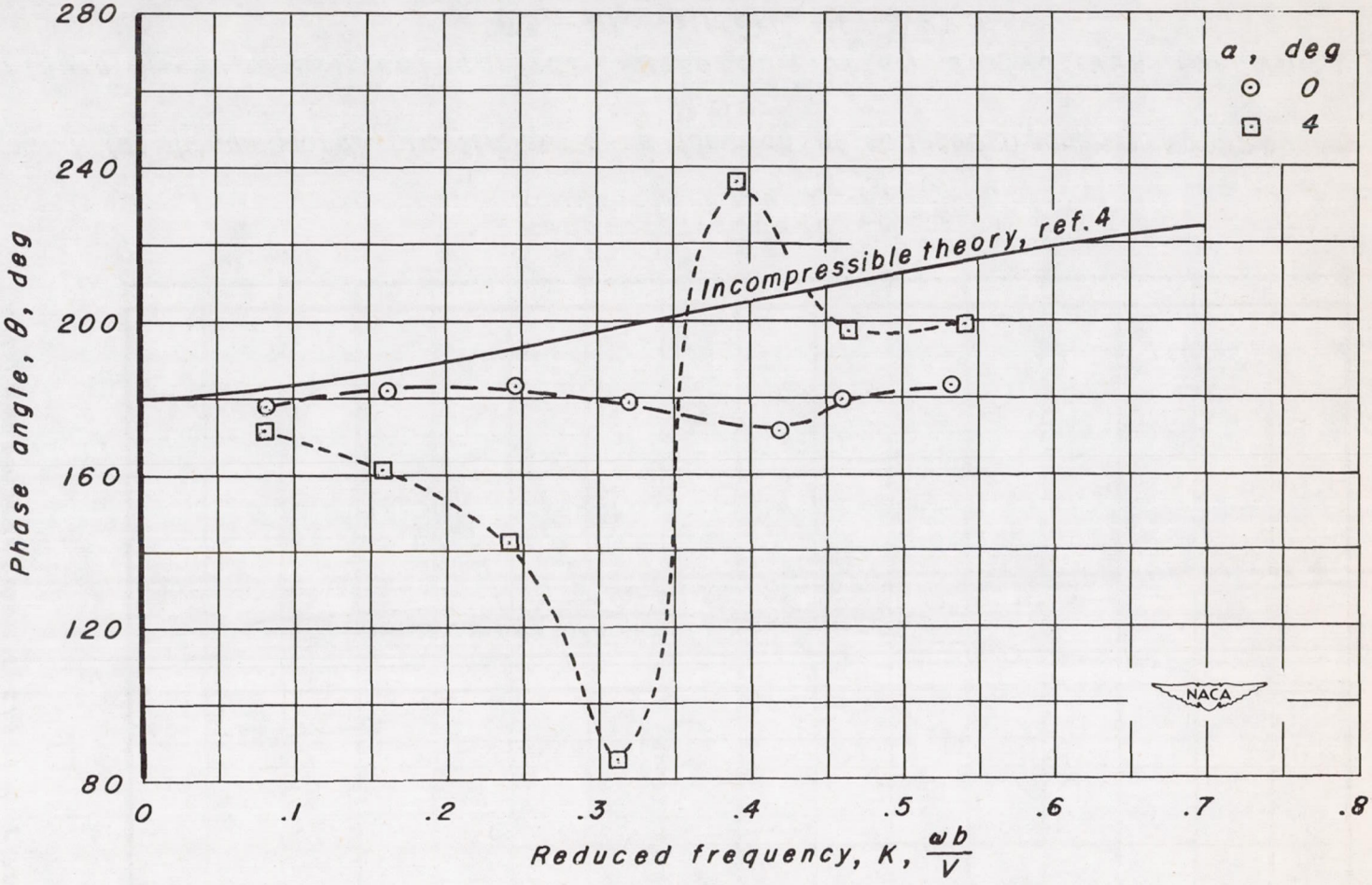

(b) Phase angle of hinge-moment coefficient as a function of reduced frequency. M, 0.725

Figure 8.- Continued.

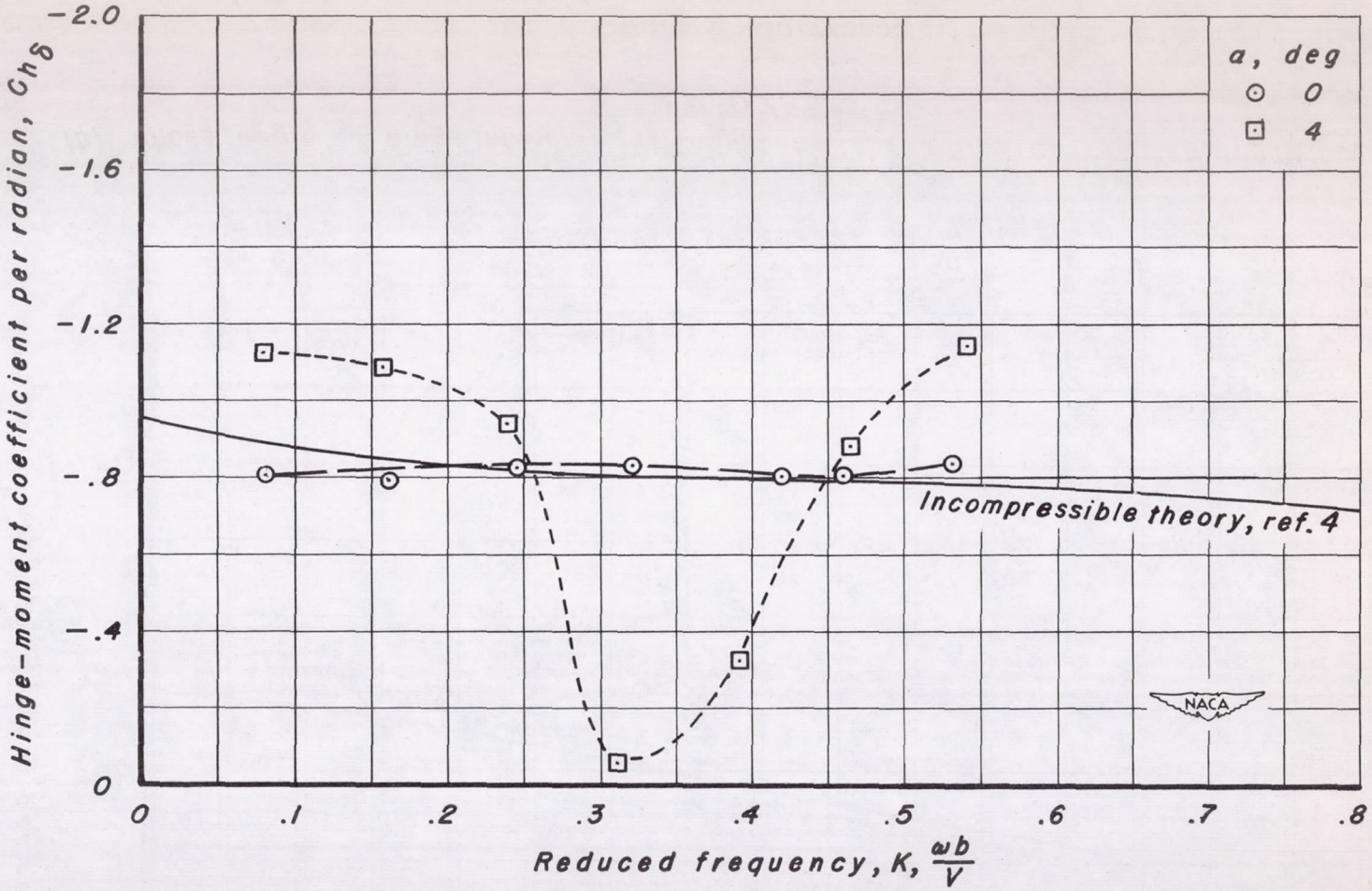

(c) Real component of hinge-moment coefficient as a function of reduced frequency. M, 0.725

Figure 8.-Continued.

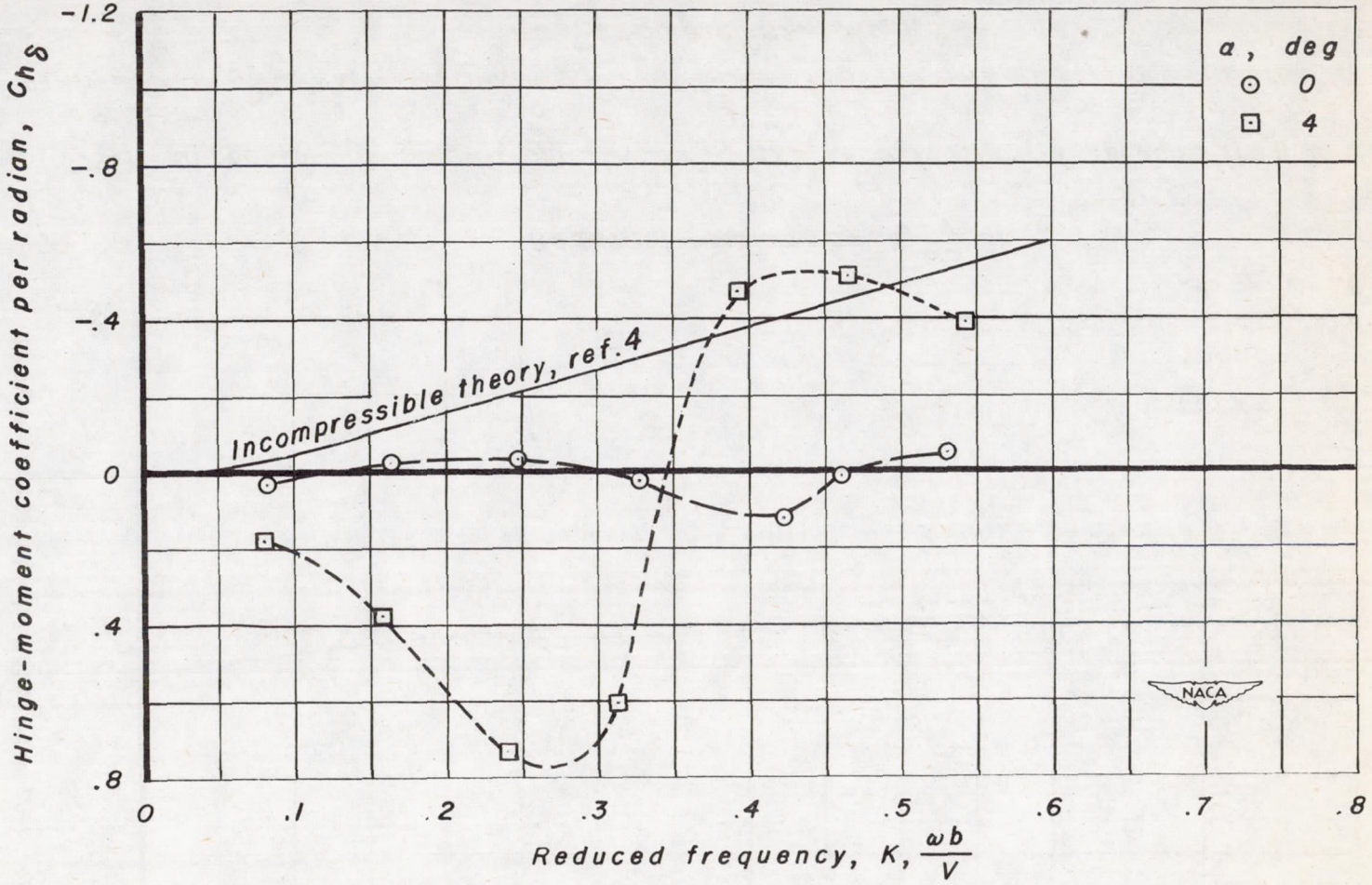

(d) Imaginary component of hinge-moment coefficient as a function of reduced frequency. M, 0.725

Figure 8.- Concluded.

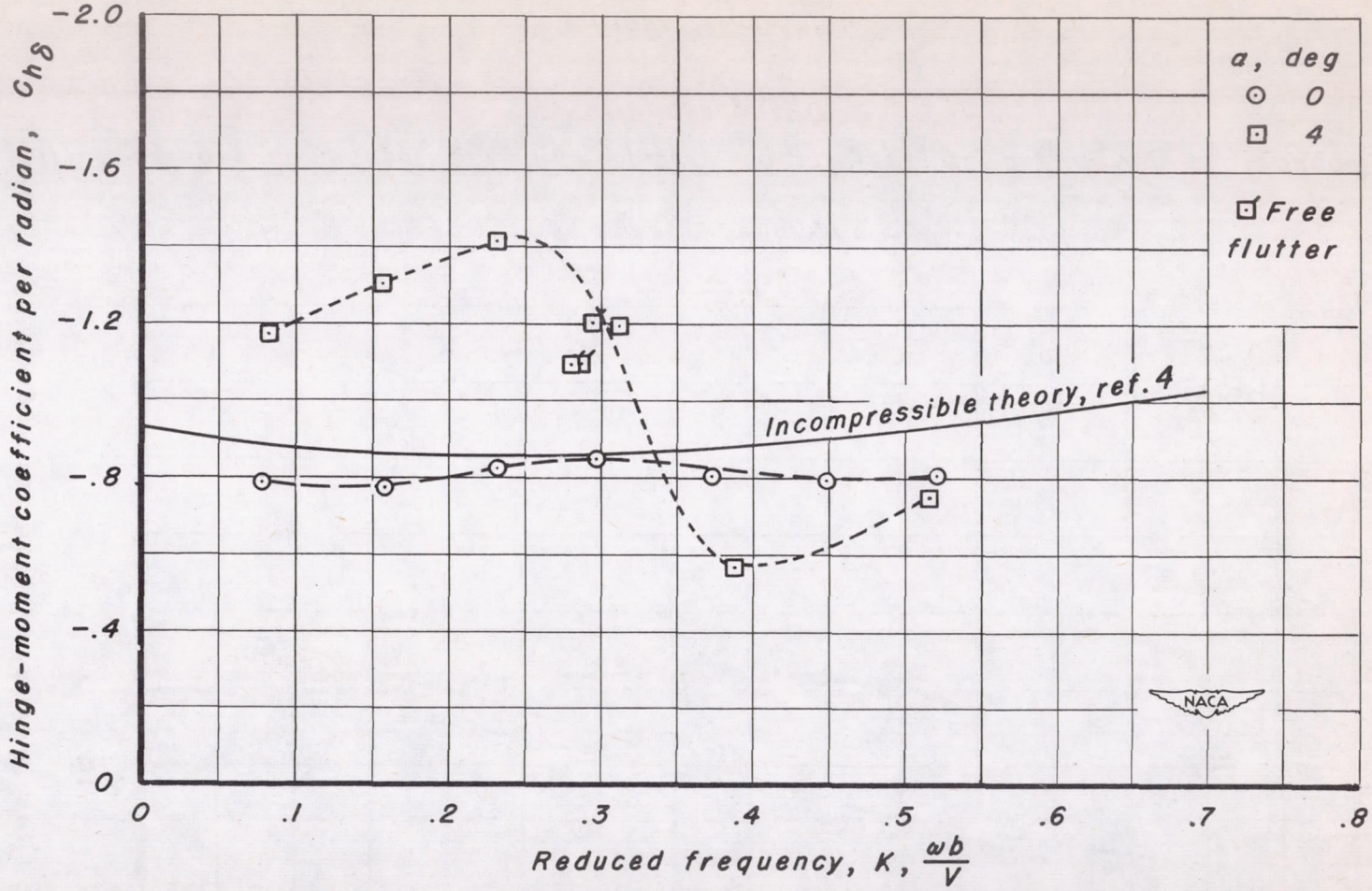

(a) Hinge-moment coefficient as a function of reduced frequency M,0.75

Figure 9.—Supercritical control-surface flutter derivatives for NACA 65_1-213 airfoil. M, 0.75

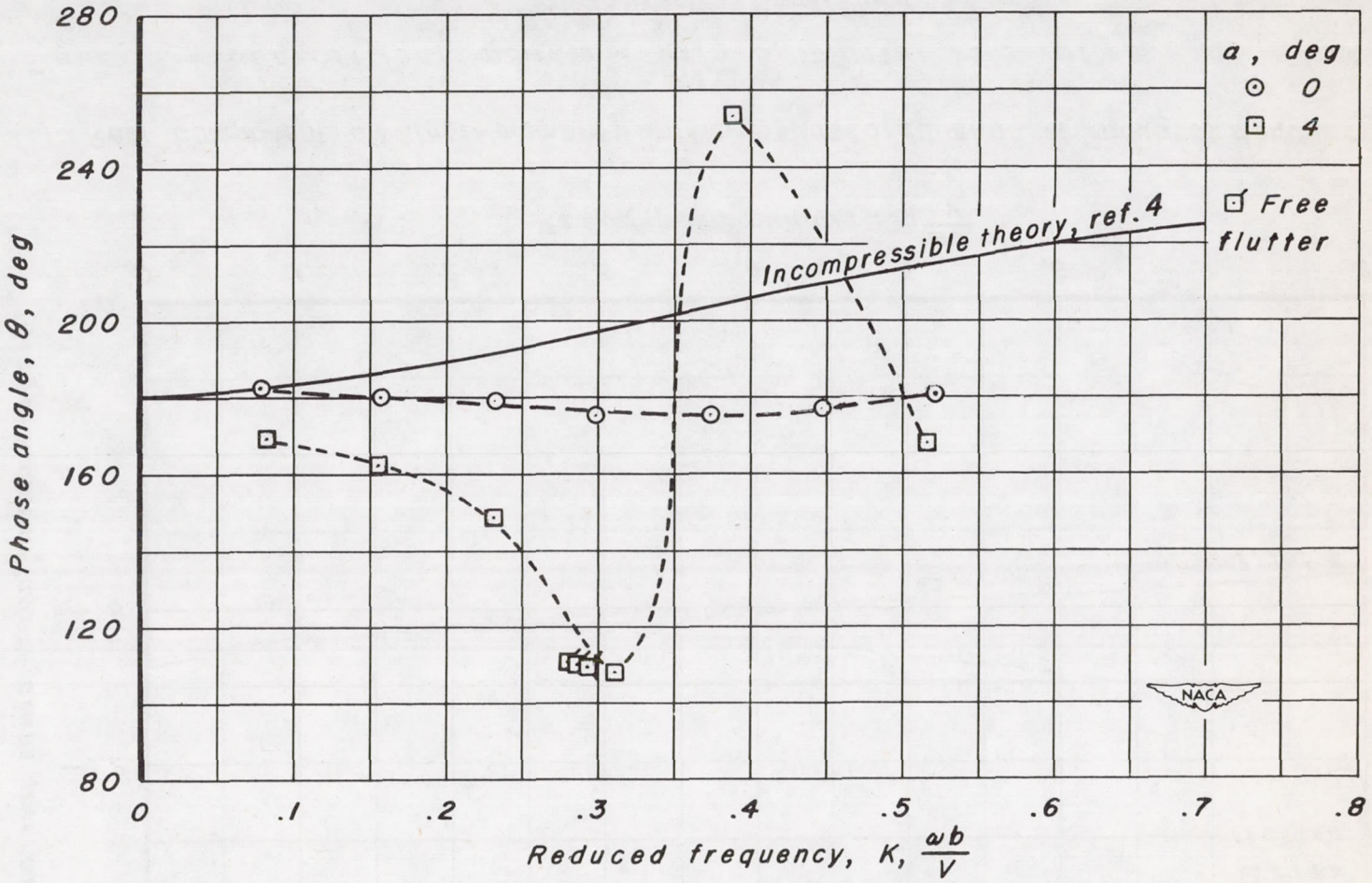

(b) Phase angle of hinge-moment coefficient as a function of reduced frequency. M,0.75

Figure 9.—Continued.

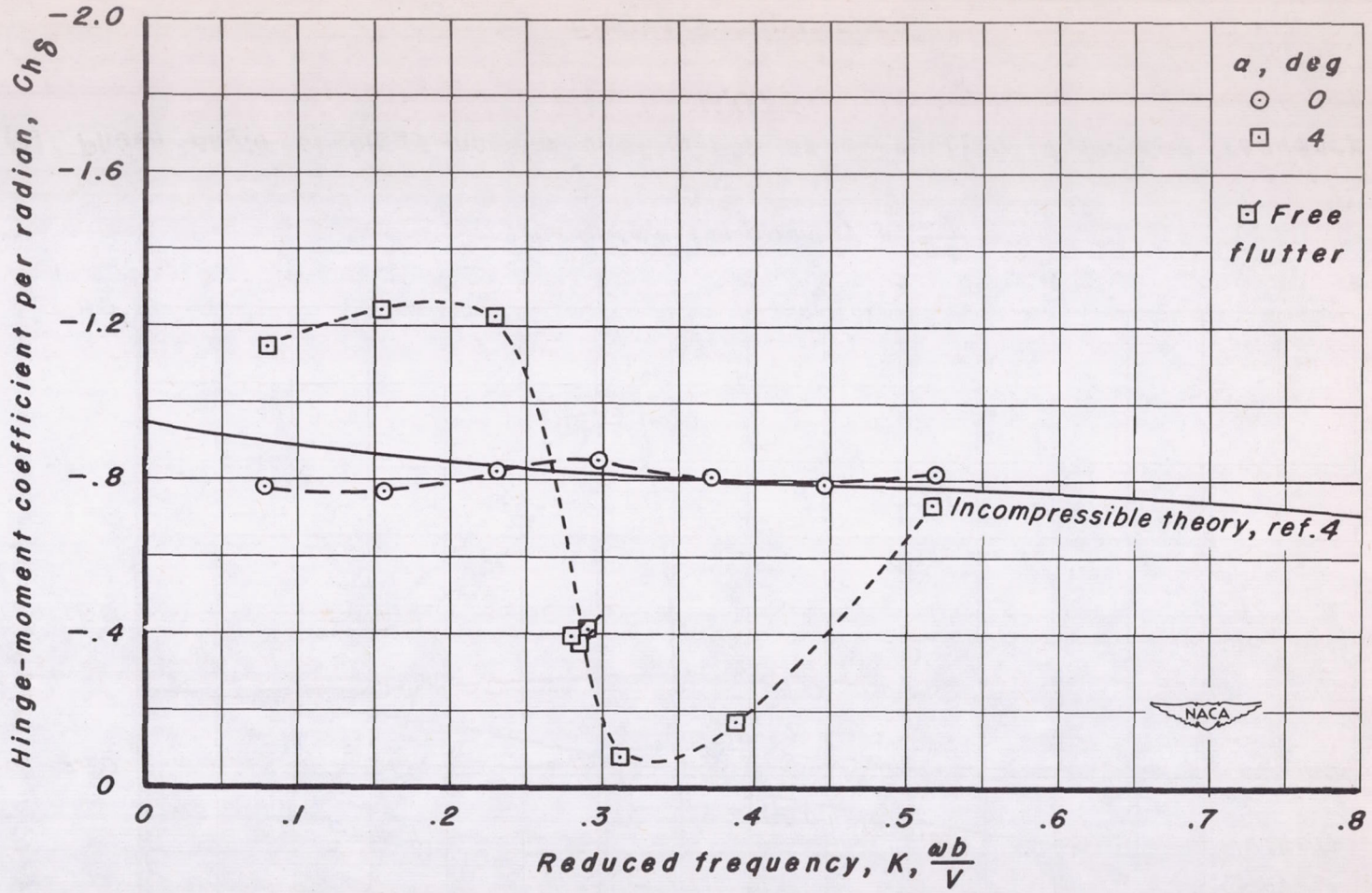

(c) Real component of hinge-moment coefficient as a function of reduced frequency.

M, 0.75

Figure 9.—Continued.

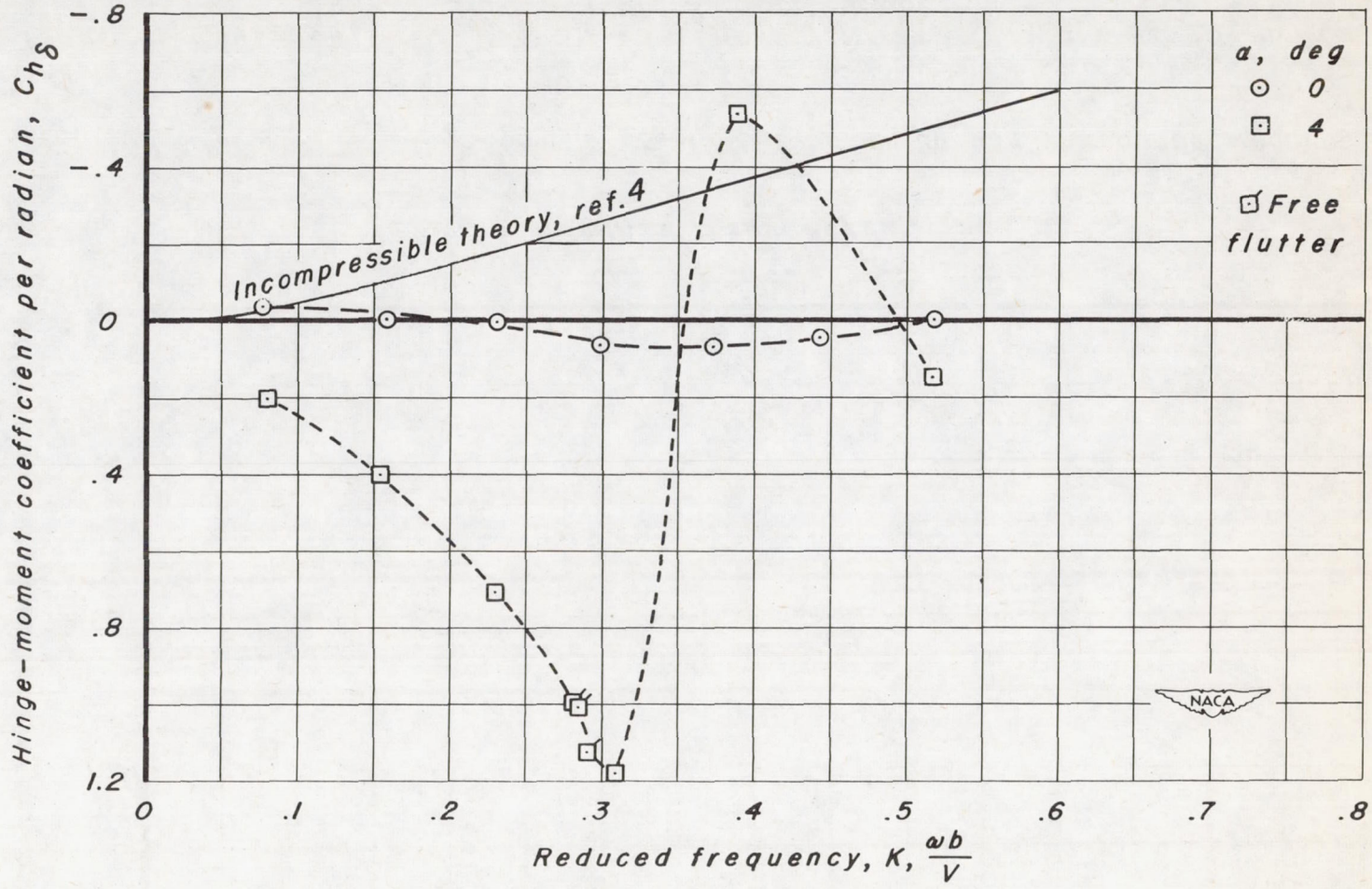

(d) Imaginary component of hinge-moment coefficient as a function of reduced frequency. M, 0.75

Figure 9.—Concluded.

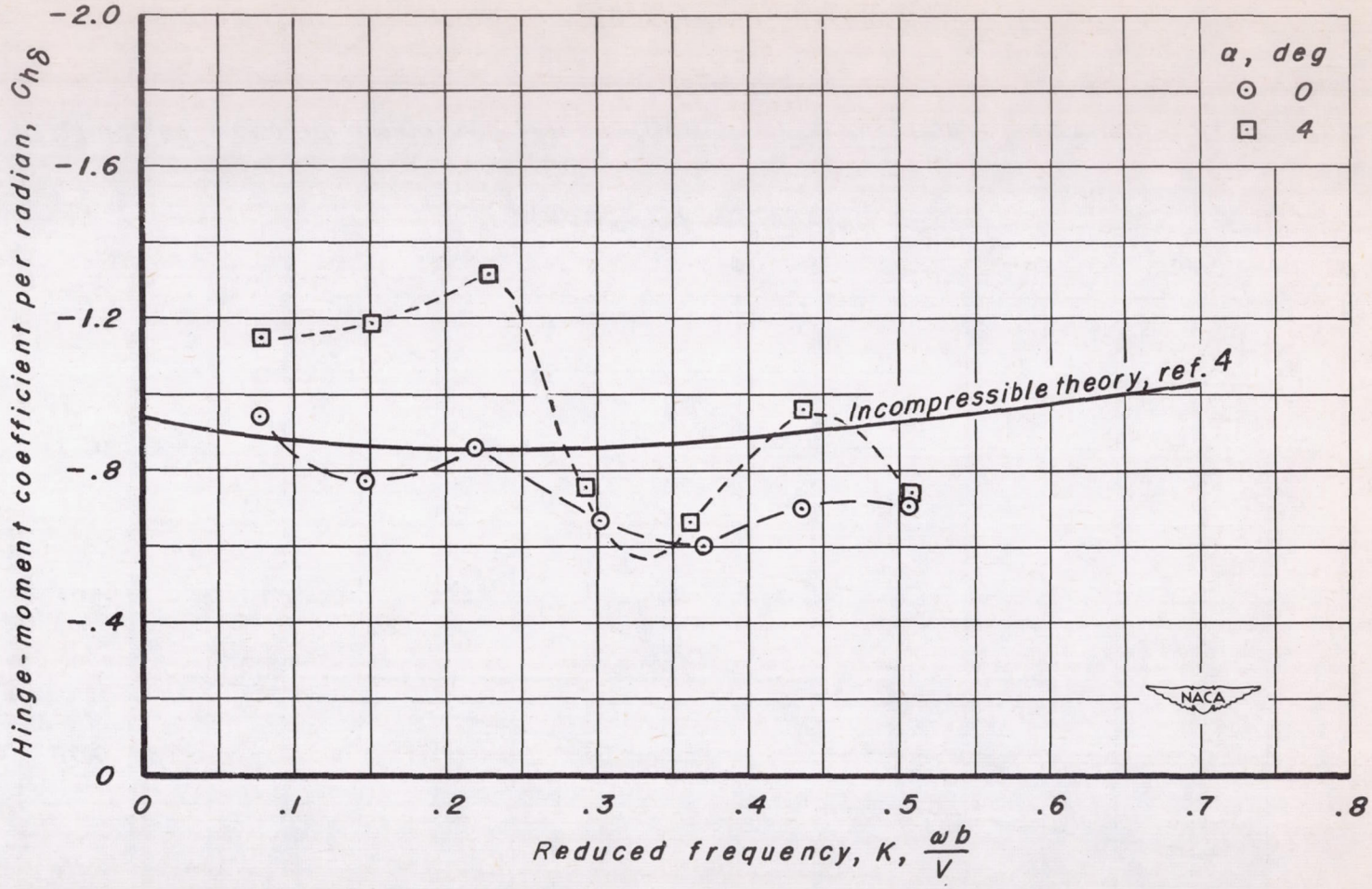

(a) Hinge-moment coefficient as a function of reduced frequency. M,0.775

Figure 10.–Supercritical control-surface flutter derivatives for NACA 65_1–213 airfoil. M, 0.775

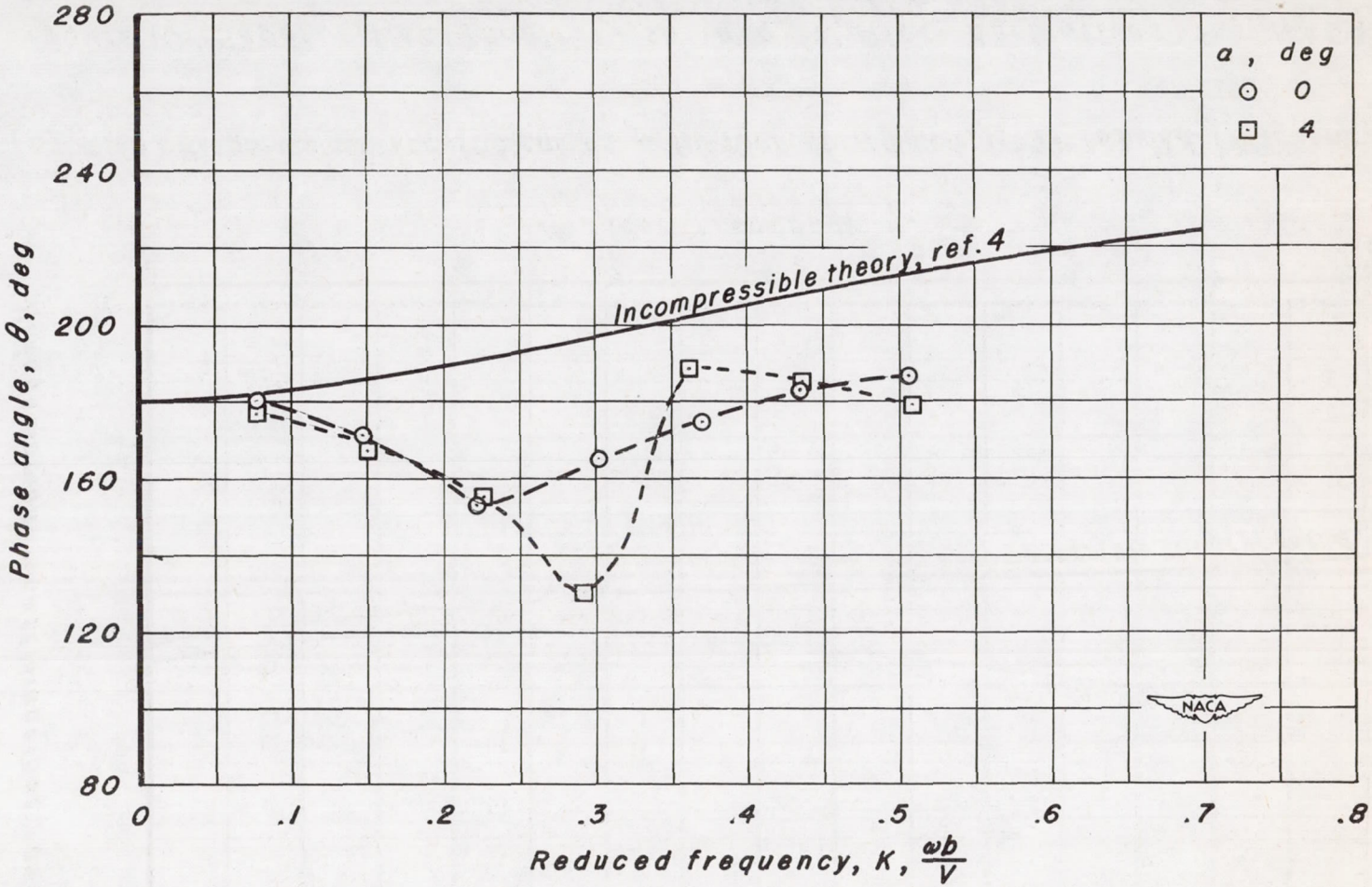

(b) Phase angle of hinge-moment coefficient as a function of reduced frequency. M,0.775

Figure 10.—Continued.

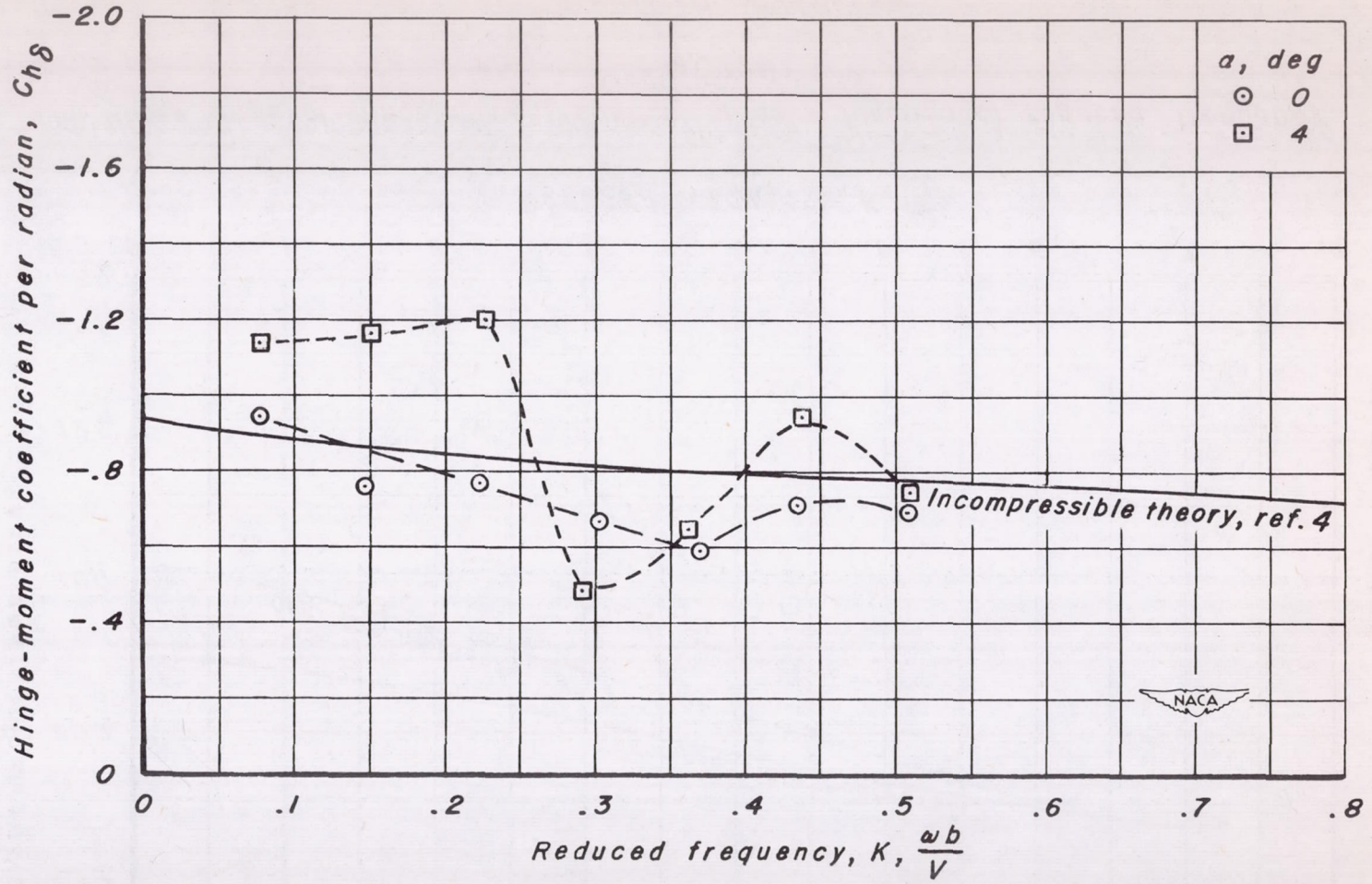

(c) Real component of hinge-moment coefficient as a function of reduced frequency.

M,0.775

Figure 10.–Continued.

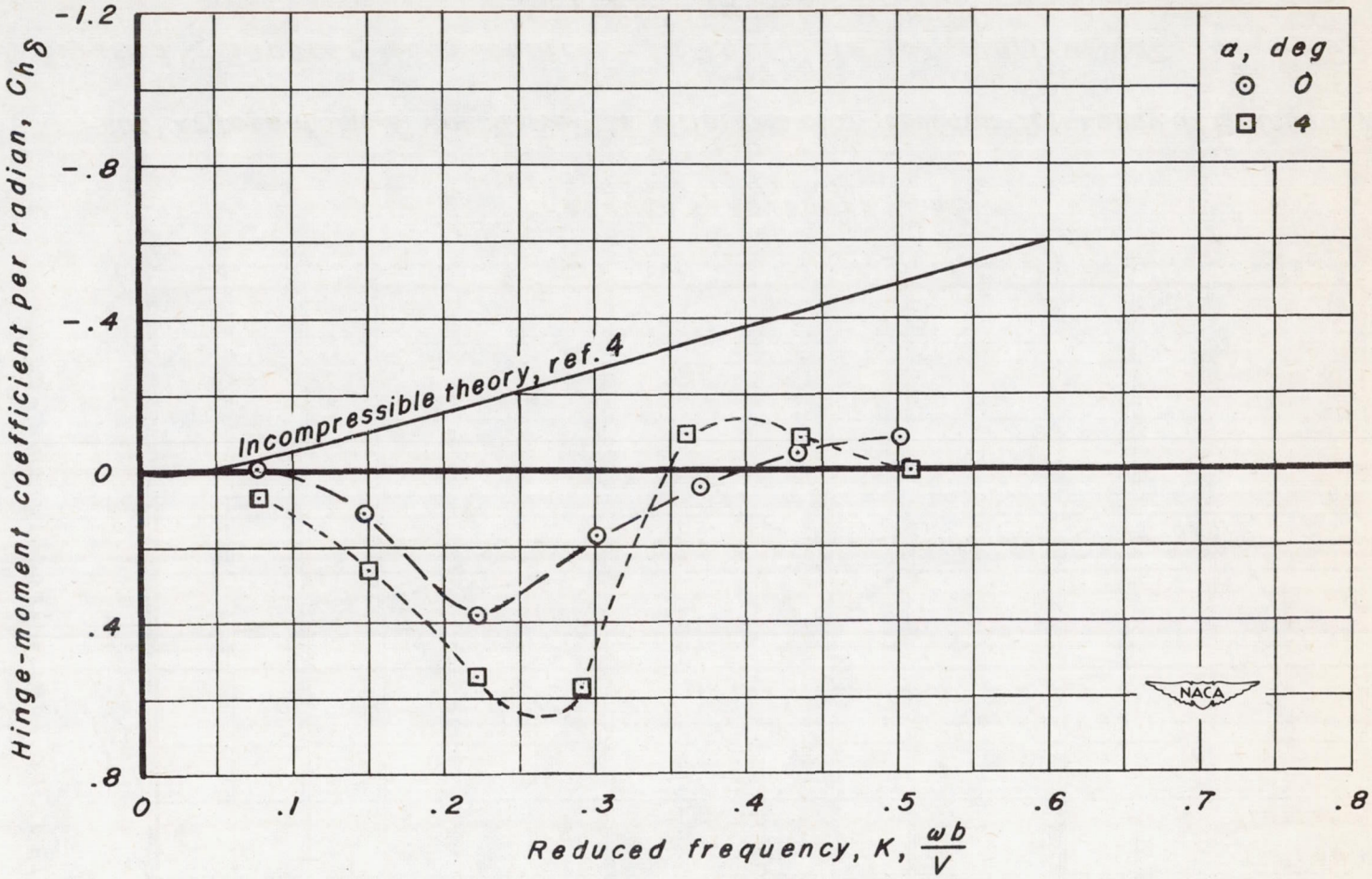

(d) Imaginary component of hinge-moment coefficient as a function of reduced frequency. M,0775

Figure 10.–Concluded.

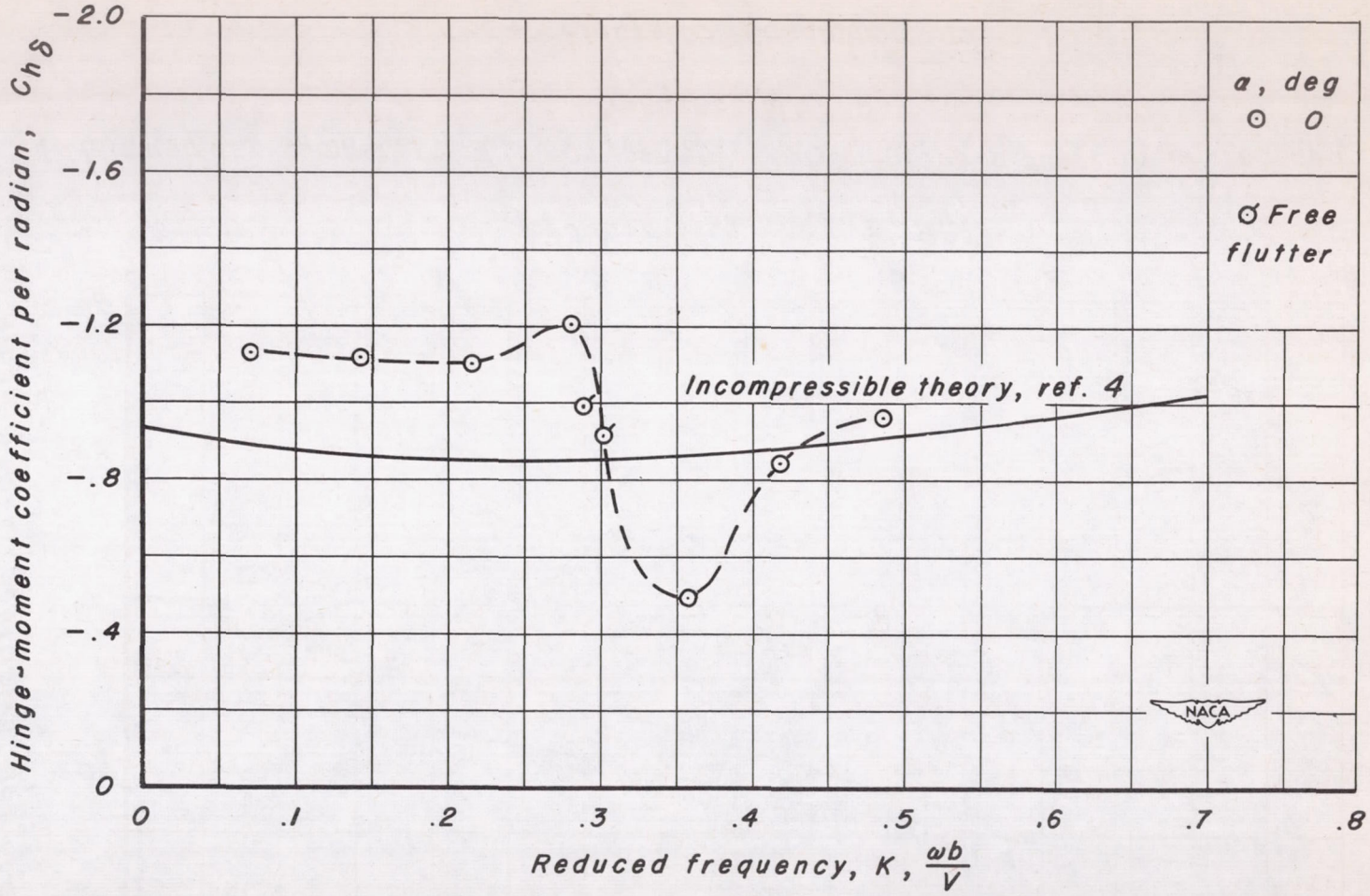

(a) Hinge-moment coefficient as a function of reduced frequency. M,0.80

Figure 11.–Supercritical control–surface flutter derivatives for NACA 65_1–213 airfoil. M, 0.80

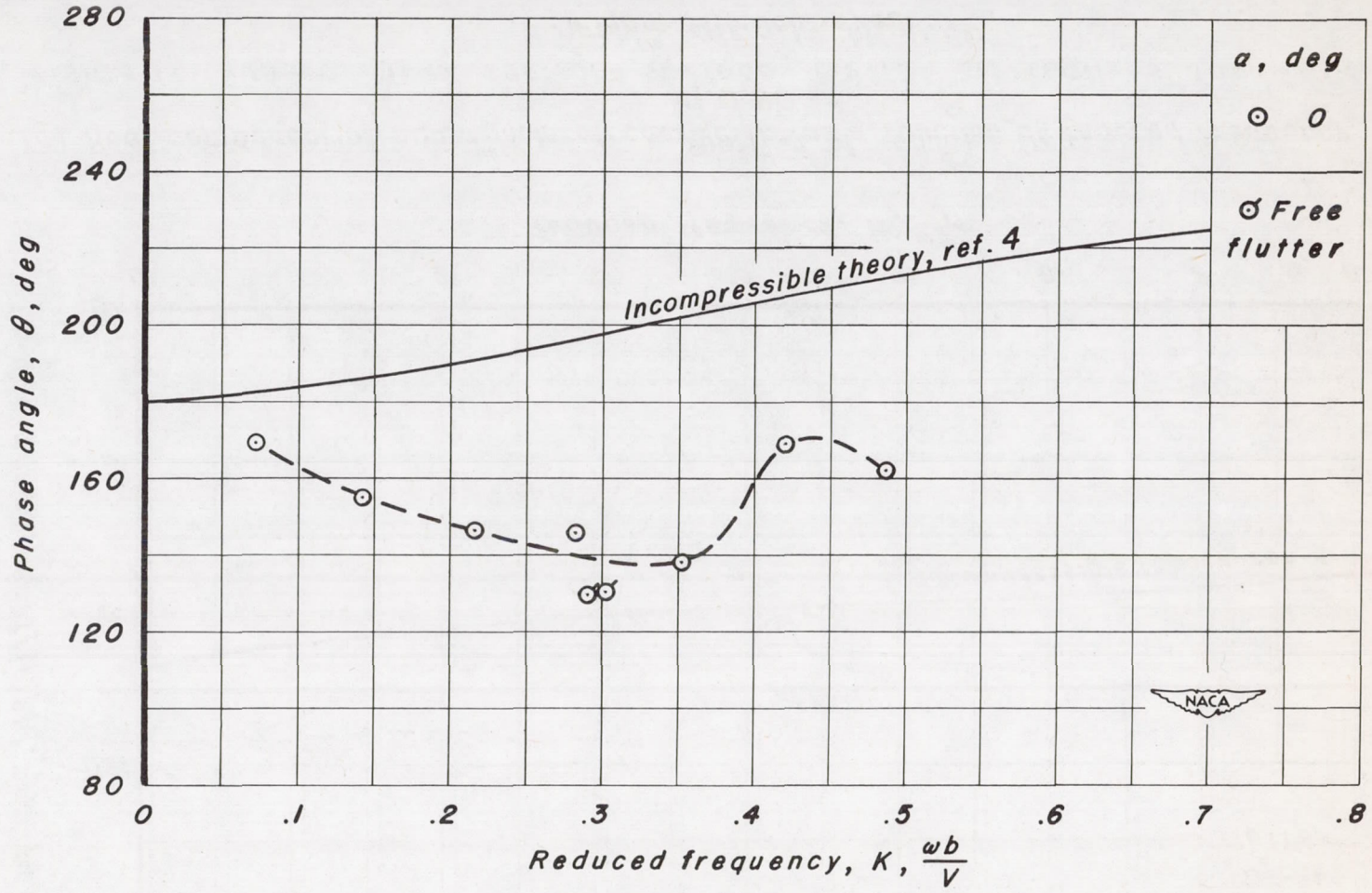

(b) Phase angle of hinge-moment coefficient as a function of reduced frequency. M, 0.80

Figure 11.—Continued.

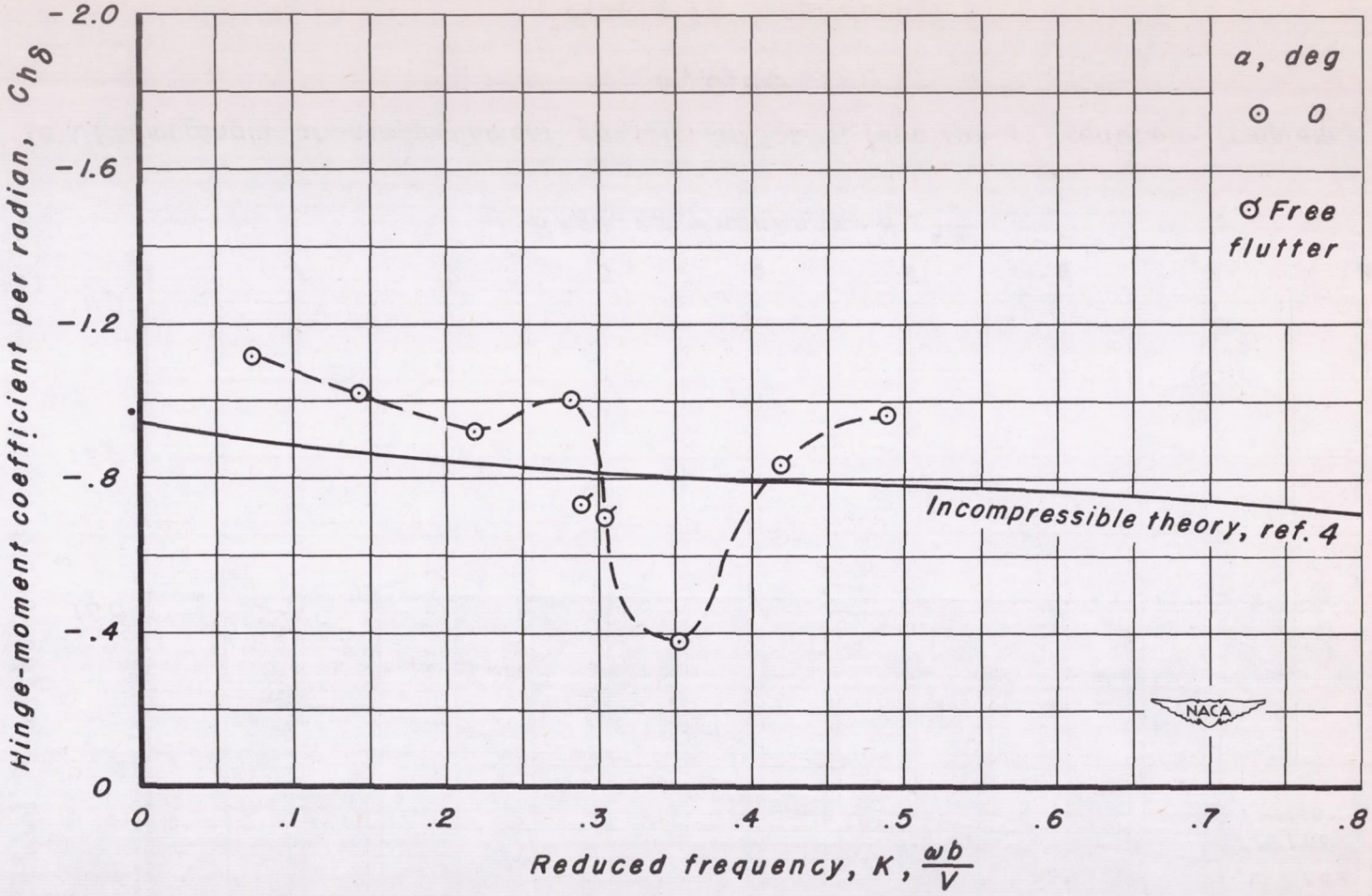

(c) Real component of hinge-moment coefficient as a function of reduced frequency. M, 0.80

Figure 11.—Continued.

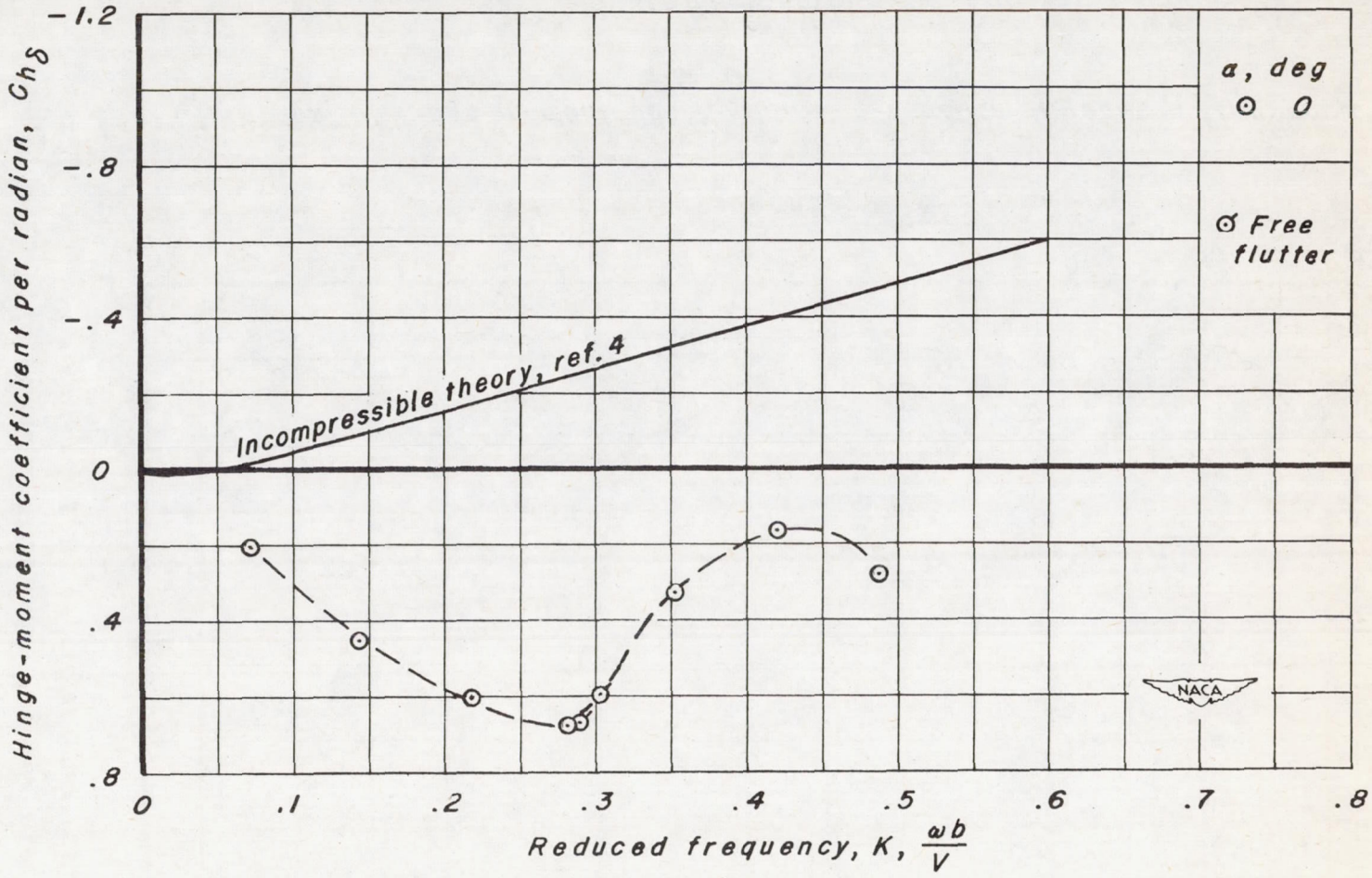

(d) Imaginary component of hinge-moment coefficient as a function of reduced frequency. M, 0.80

Figure 11.— Concluded.

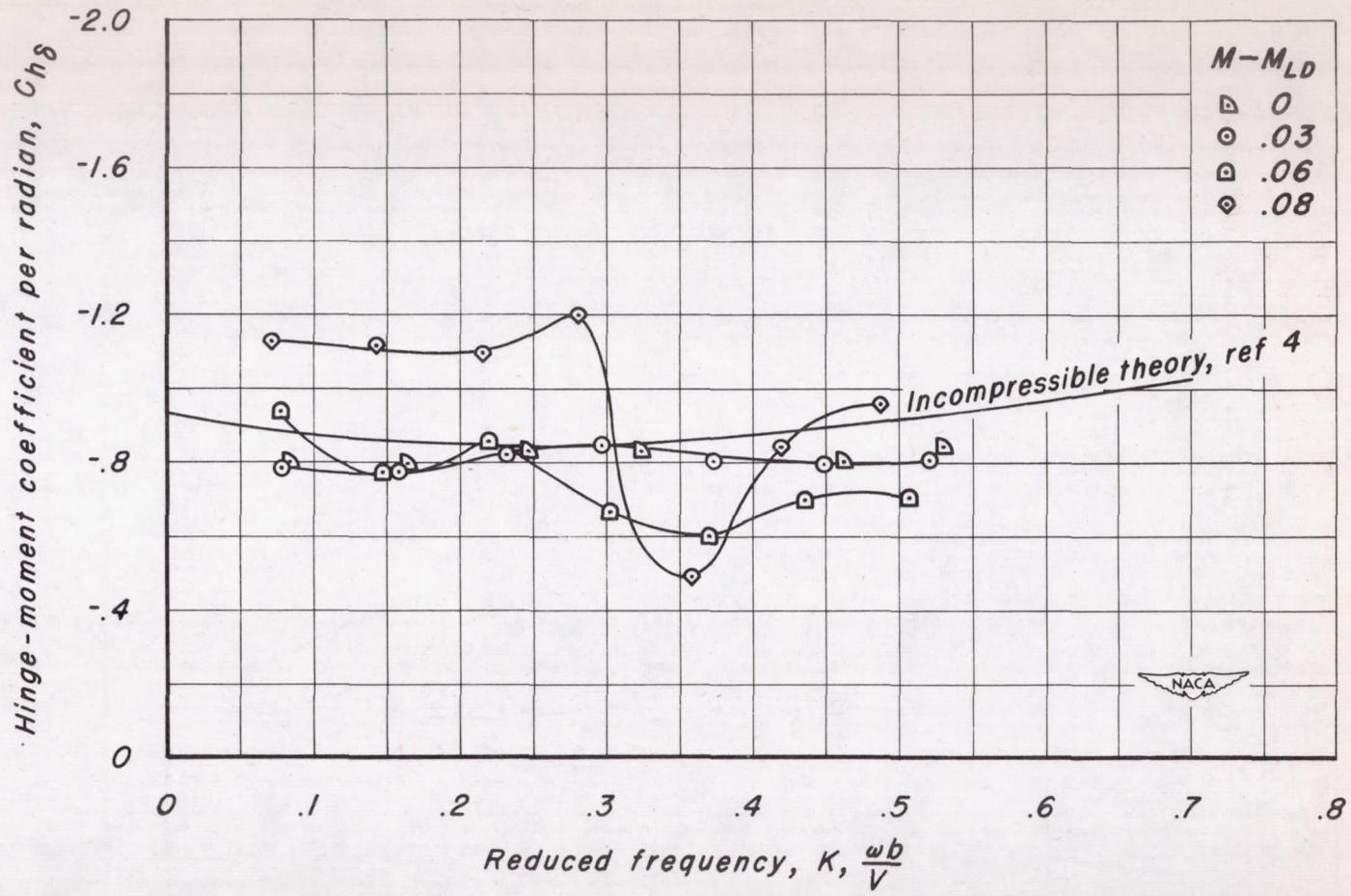

(a) Hinge-moment coefficient as a function of reduced frequency for Mach number increments above the Mach number for lift divergence. α, 0°

Figure 12.–Summary of supercritical control-surface flutter derivatives. α, 0°

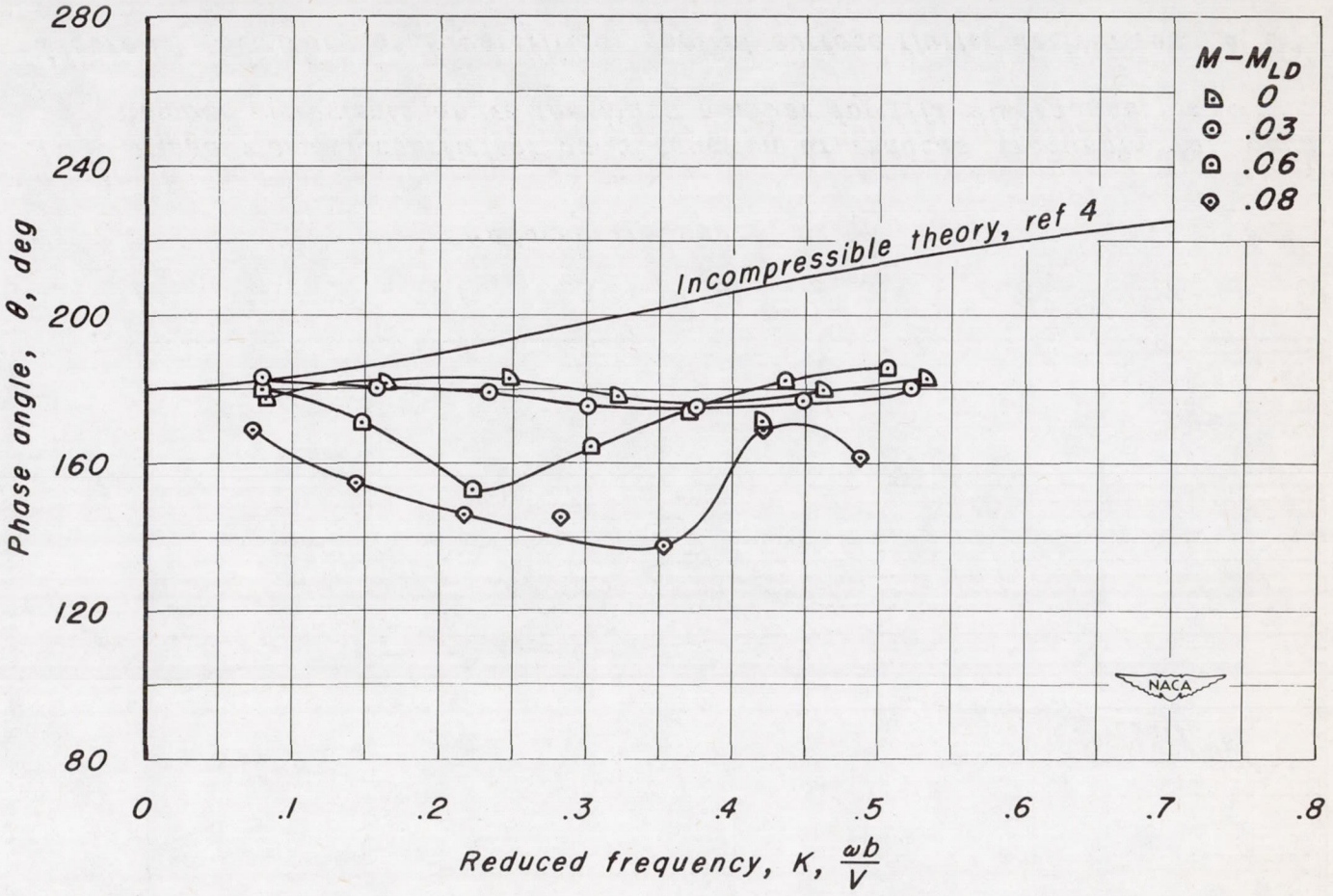

(b) Phase angle of hinge-moment coefficient as a function of reduced frequency for Mach number increments above the Mach number for lift divergence. α, 0°

Figure 12.–Concluded.

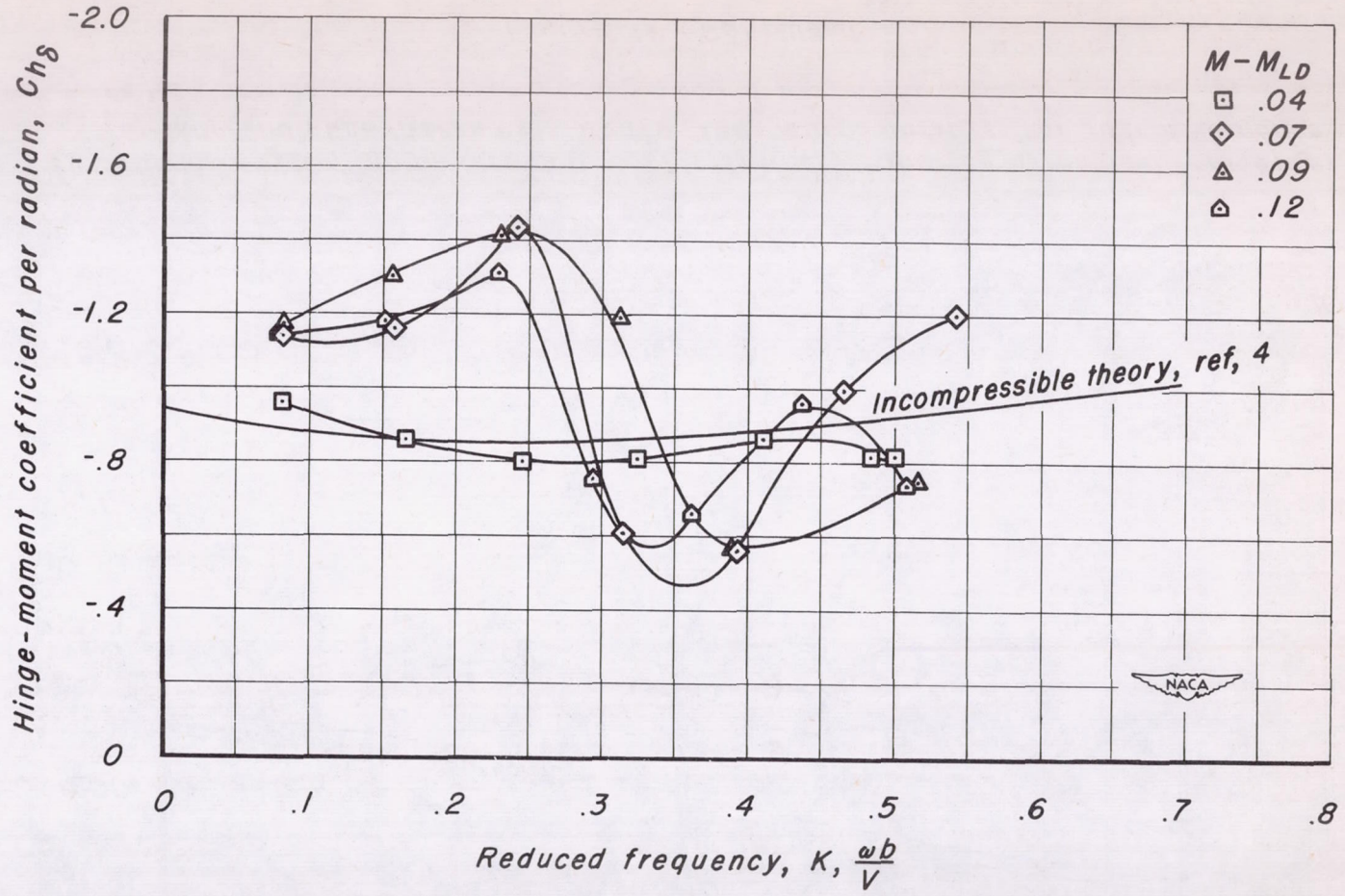

(a) Hinge-moment coefficient as a function of reduced frequency for Mach number increments above the Mach number for lift divergence. α, 4°

Figure 13.—Summary of supercritical control-surface flutter derivatives for NACA 65_1-213 airfoil. α, 4°

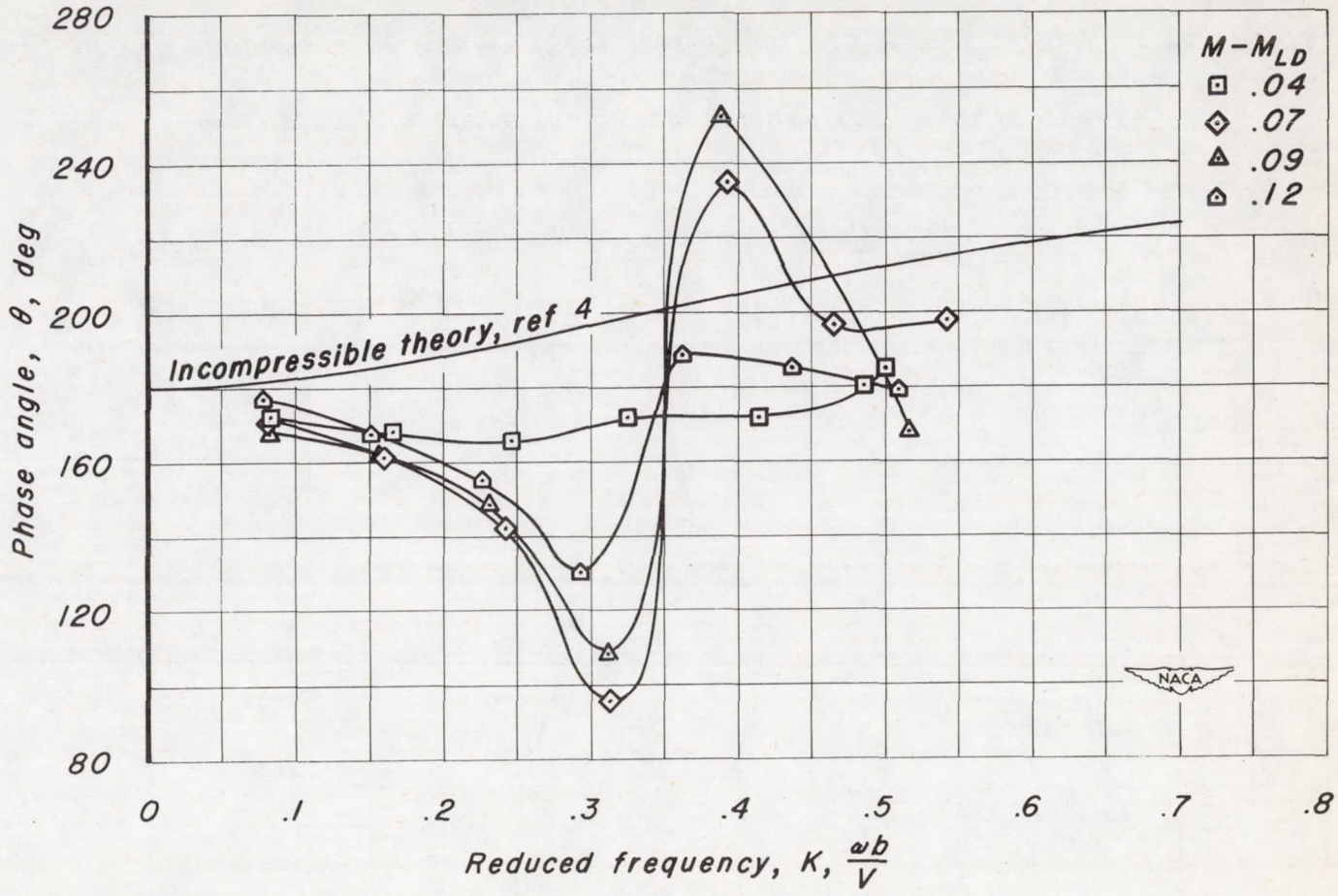

(b) Phase angle of hinge-moment coefficient as a function of reduced frequency for Mach number increments above the Mach number for lift divergence. α, 4°

Figure 13.—Concluded.